OAK RIDGE
NATIONAL LABORATORY
MANAGED BY UT-BATTELLE
FOR THE DEPARTMENT OF ENERGY

ORNL/TM-2012/177

# Final Report

# Nano Catalysts for Diesel Engine Emission Remediation

## April 2012

**Prepared by**

**Chaitanya K. Narula**
**Xiaofan Yang**
**Melanie Moses-DeBusk**
**David R. Mullins**
**Shannon M. Mahurin**
**Zili Wu**

UT-BATTELLE
ORNL-27 (4-00)

ORNL/TM-2011/177

Industrial Technology Program – Nano-manufacturing

# FINAL REPORT

# NANO CATALYST FOR DIESEL ENGINE EMISSION REMEDIATION

Chaitanya K. Narula
Xiaofan Yang
Melanie Moses-DeBusk
David R. Mullins
Shannon M. Mahurin
Zili Wu

Date Published: April 2012

Prepared by
OAK RIDGE NATIONAL LABORATORY
Oak Ridge, Tennessee 37831-6283
managed by
UT-BATTELLE, LLC
for the
U.S. DEPARTMENT OF ENERGY
under contract DE-AC05-00OR22725

**CONTENTS**

**Page**


LIST OF FIGURES ..... iiv
LIST OF ACRONYMS ..... vi
ACKNOWLEDGEMENTS ..... viiii
EXECUTIVE SUMMARY ..... ix
1. INTRODUCTION ..... 1-4
   1.1 OBJECTIVE ..... 1
   1.2 PREVIOUS STUDIES ..... 2
   1.3 APPROACH ..... 3
2. CATALYST SYNTHESIS & TESTS PROTOCOLS ..... 4-7
   2.1 SYNTHESIS ..... 2-7
   2.2 DEGREENING AND $NO_X$ CONVERSION EFFICIENCY ..... 6
   2.3 AGING PROTOCOL ..... 7
3. CATALYST CHARACTERIZATION ..... 8-11
   3.1 ZSM-5 TYPE HETEROBIMETALLIC ZEOLITES ..... 8
   3.2 SSZ-13 TYPE HETEROBIMETALLIC ZEOLITES ..... 11
4. NOX CONVERSION EFFICIENCY ..... 12-19
   4.1 BORON SUBSTITUTED CU-ZSM-5 ..... 12
   4.2 IRON SUBSTITUTED CU-ZSM-5 ..... 13
   4.3 HETEROBIMETALLIC ZEOLITES ..... 14
   4.2 IGENERALIRTY OF ION EXCAHNGE SYNTHESIS OF HETEROBIMETALLIC ZEOLITES ..... 16
   4.2 EFFECTS OF ZEOLITE FRAMEWORK ..... 17
   4.2 IMPCAT OF NO2:NOX RATIO ..... 18
   4.2 HYDROTHHERMAL STABILTIY ..... 19
5. MECHANISTIC STUDIES ..... 20-26
6. CONCLUSIONS ..... 27
7. COMMERCIALIZATION ..... 28
8. PUBLICATIONS ..... 29
9. REFERENCES ..... 30-31

## LIST OF FIGURES


| Figure | | Page |
|---|---|---|
| 1.1 | Figure 1: Left – MFI type zeolite frame-work of ZSM-5; Right Chabazite type framework of SSZ-13 | 2 |
| 2.1 | Schematics and picture of the bench-top reactor fitted with Innova 1314 gas analyzer (California Analytical Instruments, Inc.) monitored $NH_3$, $CO_2$, $N_2O$, and $H_2O$, a chemiluminescence 600 HCLD analyzer (California Analytical Instruments, Inc.) monitored NO/$NO_x$, and $O_2$ was monitored by a Rosemount NGA 2000 Multi-Component gas analyzer using a paramagnetic oxygen sensor. | 7 |
| 3.1 | Powder XRD of ZSM-5 based catalyst | 8 |
| 3.2 | Diffuse reflectance UV-Vis (A) and EPR (B) of Cu-ZSM-5, Fe-ZSM-5, and CuFe-ZSM-5. | 9 |
| 3.3 | XANES and EXAFS of Cu-ZSM-5 and CuFe-ZSM-5 | 10 |
| 3.4 | Powder XRD of zeolite Y, SSZ-13, Cu-SSZ-13 and CuFe-SSZ-13 | 11 |
| 4.1 | $NO_x$ conversion efficiency of Cu-ZSM-5 and Fe-ZSM-5 tested with simulated off-road diesel engine exhaust. The performance of a physical mixture (1:1) of Cu-ZSM-5 and Fe-ZSM-5 is simulated as an average of the tested results from the two catalysts in black dashed line. | 12 |
| 4.2 | $NO_x$ conversion on Cu-BZSM-5 vs. Cu-ZSM-5 (right) | 13 |
| 4.3 | Ammonia-SCR $NO_x$ conversion over Cu-ZSM-5, CuFe-ZSM-5, and Cu-[FeZSM-5]51 | 14 |
| 4.4 | NOx conversion efficiency (A) and N2O production (B) patterns of CuFe-ZSM-5 compared to that of Cu-ZSM-5 and Fe-ZSM-5 tested with simualted off-road diesel engine exhaust. | 15 |
| 4.5 | NOx conversion efficiency vs. NH3 consumption ratio with a cutoff value set at 90% to track NOx conversion over Cu-ZSM-5, CuFe-ZSM-5, and Cu-[FeZSM-5]51 to track the "Fast SCR Reaction": 2NH3 + NO2 + NO → N2 + H2O . | 15 |
| 4.6 | $N_2$ formation selectivity, defined as (reduced_$NO_x$ – $N_2O$_production)/ reduced_$NO_x$, of catalyst Cu-ZSM-5, Fe-ZSM-5, and CuFe-ZSM-5 (Left). $NO_x$ conversion in the absence of $NH_3$ over CuFe-ZSM-5 under the following condition: 8.5% $O_2$; 8% $CO_2$; 7.25% $H_2O$; 250 ppm NO; 250 ppm $NO_2$ with $N_2$ as balance (Right) | 16 |
| 4.7 | $NO_x$ conversion efficiency of CuM-ZSM-5 (M = Sc, Fe, In, and La) compared to that of Cu-ZSM5 and Fe-ZSM5 tested with simulated off-road diesel engine exhaust. | 17 |
| 4.8 | NOx conversion efficiency of (A): CuFe-ZSM-5, Cu-Beta, and CuFe-Beta; (B) CuFe-ZSM-5, Cu-SSZ-13, and CuFe-SSZ-13. | 18 |
| 4.9 | $NO_x$ conversion efficiency of CuFe-SSZ-13 at 160ºC and 195ºC as a function of $NO_2/NO_x$ ratio. | 18 |
| 4.10 | $NO_x$ SCR comparison of Cu-ZSM-5, Fe-ZSM-5, and CuFe-ZSM-5 after hydrothermal aging. | 19 |
| 5.1 | DRIFTS spectra of Cu-SSZ-13 at 150°C during the 4-step treatment (A. $NO_x/O_2$ flow, B. He purging, C. $NH_3/O_2$ flow, and D. desorption in He with temperature ramping to 600°C. Each step takes 15 minutes). | 20 |
| 5.2 | DRIFTS spectra of Cu-SSZ-13 at 150°C under a flow of NO (250 ppm) and He (balance) for 15 minutes. | 21 |
| 5.3 | DRIFTS spectra of $NO^+$ and nitrite/nitrate adsorbed over Cu-SSZ-13 during the heating process from 150°C to 500°C (20°C/min) under a flow of He. Time interval between two spectra is 0.02 minute | 21 |

5.4 DRIFTS spectra comparison of Cu-SSZ-13 between two conditions: (1) a flow of NH3 (500 ppm) and He (balance) for 15 minutes (dotted line) and (2) the third step treatment of NH3 (500 ppm), O2 (8.5%), and He (balance) for 15 minutes (solid line). ..... 22
5.5 DRIFTS spectra of Cu-SSZ-13 at 250°C under the 4-step treatment (A. $NO_x/O_2$ flow, B. He purging, C. $NH_3/O_2$ flow, and D. desorption in He with temperature ramping to 600°C. Each step takes 15 minutes). ..... 23
5.6 DRIFTS spectra of CuFe-SSZ-13 vs. Cu-SSZ-13 treated by $NO_x/O_2$ at 150°C ..... 24
5.7 DRIFT spectra of CuFe-SSZ-13 at 150°C during the 4-step treatment (A. $NO_x/O_2$ flow, B. He purging, C. $NH_3/O_2$ flow, and D. desorption in He with temperature ramping to 600°C. Each step takes 15 minutes). ..... 24
5.8 DRIFTS spectra of CuFe-SSZ-13 at 250°C under the 4-step treatment (A. $NO_x/O_2$ flow, B. He purging, C. $NH_3/O_2$ flow, and D. desorption in He with temperature ramping to 600°C. Each step takes 15 minutes). ..... 25

## LIST OF ACRONYMS

| | |
|---|---|
| DOE | U.S. Department of Energy |
| EPA | Environmental Protection Agency |
| EPR | Electron Paramagnetic Resonance |
| EXAFS | Extended X-ray Absorption Fine Structure |
| FCC | Fluid Catalytic Cracking |
| NOx | Nitrogen Oxides |
| SCR | Selective Catalytic Reduction |
| XANES | X-ray Absorption Near Edge Structure |

## ACKNOWLEDGEMENTS

This research is sponsored by the U.S. Department of Energy, Office of Energy Efficiency and Renewable Energy, Industrial Technologies Program, under contract DE-AC05-00OR22725 with UT-Battelle, LLC. The IR work was performed at the Center for Nanophase Materials Sciences, which is sponsored at Oak Ridge National Laboratory by the Scientific User Facilities Division, Office of Basic Energy Sciences, and U.S. Department of Energy. The in-kind support from John Deere and technical discussions with Dr. Danan Dou are gratefully acknowledged.

Authors thank Dr. M. Kidder and Dr. G. Brown for assistance in UV-VIS data acquisition. Dr. D. Mullins carried out EXAFS & XANES experiments, Dr. Mahurin EPR work, and Dr. Z. Wu assisted with DRIFTS experiments for mechanistic studies

We thank Drs. Joseph Renk, Gideon Varga, and Elmer Fleischman for supporting this activity and providing valuable input. We also thank Drs. Craig Blue and Ron Ott, Field Technical Mangers at ORNL for their support.

## EXECUTIVE SUMMARY

The objective of this project was to develop durable zeolite nanocatalysts with broader operating temperature windows to treat diesel engine emissions to enable diesel engine based equipment and vehicles to meet future regulatory requirements. A second objective was to improve hydrothermal durability of zeolite catalysts to at least 675°C. The results presented in this report show that we have successfully achieved both objectives.

Since it is accepted that the first step in $NO_x$ conversion under SCR (selective catalytic reduction) conditions involves NO oxidation to $NO_2$, we reasoned that catalyst modification that can enhance NO oxidation at low-temperatures should facilitate $NO_x$ reduction at low temperatures. Considering that Cu-ZSM-5 is a more efficient catalyst than Fe-ZSM-5 at low-temperature, we chose to modify Cu-ZSM-5. It is important to point out that the poor low-temperature efficiency of Fe-ZSM-5 has been shown to be due to selective absorption of $NH_3$ at low-temperatures rather than poor NO oxidation activity. In view of this, we also reasoned that an increased electron density on copper in Cu-ZSM-5 would inhibit any bonding with $NH_3$ at low-temperatures.

In addition to modified Cu-ZSM-5, we synthesized a series of new heterobimetallic zeolites, by incorporating a secondary metal cation M ($Sc^{3+}$, $Fe^{3+}$, $In^{3+}$, and $La^{3+}$) in Cu exchanged ZSM-5, zeolite-beta, and SSZ-13 zeolites under carefully controlled experimental conditions. Characterization by diffuse-reflectance ultra-violet-visible spectroscopy (UV-Vis), X-ray powder diffraction (XRD), extended X-ray absorption fine structure spectroscopy (EXAFS) and electron paramagnetic resonance spectroscopy (EPR) does not permit conclusive structural determination but supports the proposal that $M^{3+}$ has been incorporated in the vicinity of Cu(II).

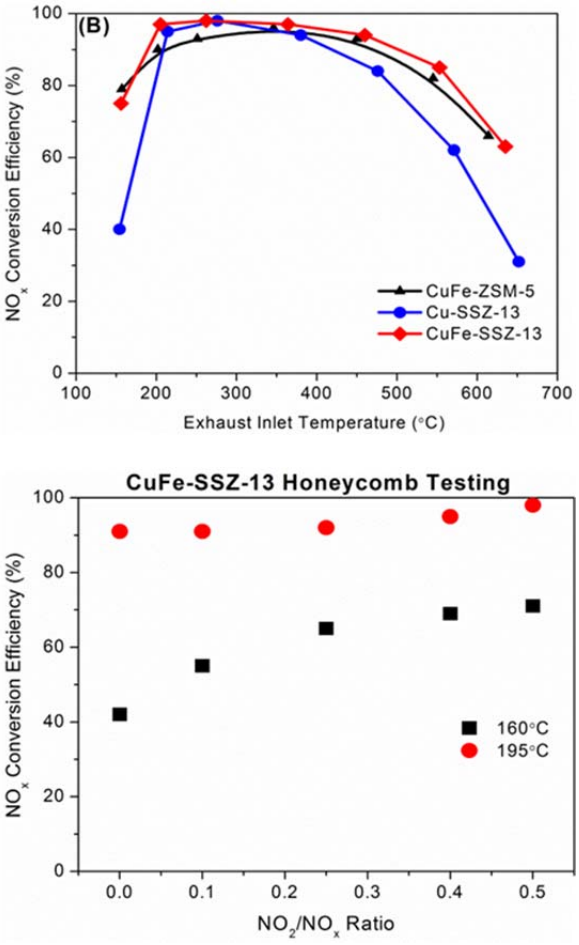


$NO_x$ Conversion by CuFe-SSZ-13 as a function of temperature (top) and as a function of $NO_2$:$NO_x$ ratio at 160 and 195°C (bottom).

The protocols for degreening catalysts, testing under various operating conditions, and accelerated aging conditions were provided by our collaborators at John Deere Power Systems.

Among various zeolites reported here, CuFe-SSZ-13 offers the best $NO_x$ conversion activity in 150-650°C range and is hydrothermally stable when tested under accelerated aging conditions. It

is important to note that Cu-SSZ-13 is now a commercial catalyst for $NO_x$ treatment on diesel passenger vehicles. Thus, our catalyst performs better than the commercial catalyst under fast SCR conditions. We initially focused on fast SCR tests to enable us to screen catalysts rapidly. Only the catalysts that exhibit high $NO_x$ conversion at low temperatures are selected for screening under varying $NO_2$:$NO_x$ ratio. The detailed tests of CuFe-SSZ-13 show that CuFe-SSZ-13 is more effective than commercial Cu-SSZ-13 even at $NO_2$:$NO_x$ ratio of 0.1.

The mechanistic studies, employing stop-flow diffuse reflectance FTIR spectroscopy (DRIFTS), suggest that high concentration of $NO^+$, generated by heterobimetallic zeolites, is probably responsible for their superior low temperature $NO_x$ activity.

The results described in this report clearly show that we have successfully completed the first step in a new emission treatment catalyst which is synthesis and laboratory testing employing simulated exhaust. The next step in the catalyst development is engine testing. Efforts are in progress to obtain follow-on funding to carry out scale-up and engine testing to facilitate commercialization of this technology.

# 1. INTRODUCTION

## 1.1 OBJECTIVE

**Our objective is to develop durable zeolite nanocatalysts with broader operating temperature windows to treat diesel engine emissions to enable diesel engine based equipment and vehicles to meet regulatory requirements. A second objective is to improve hydrothermal durability of zeolite catalysts to at least 675°C.**

The impetus for deployment of lean gasoline and diesel engines (which typically operate very lean) comes from the need to reduce emissions of $CO_2$, which is considered a major greenhouse gas. Lean burn gasoline engines also reduce fuel consumption by 6-25% and diesel engines by 20-40% as compared with stoichiometric gasoline engines. However, their deployment is inhibited by the lack of a suitable catalyst or a combination of catalysts that can selectively reduce $NO_x$ with available reductants in the engine-out exhaust to meet regulatory targets over practical driving cycles and vehicle life times. Initial hopes that copper exchanged ZSM-5 could be made sufficiently active for this process were not supported by later studies that showed conversions too low to meet regulatory requirements. For example, with a synthetic diesel fuel reductant, about 30% $NO_x$ reduction could be achieved but the fuel penalty was close to 7%.[1,2] This conversion is even less impressive when it is recognized that without injection of a reductant, the $NO_x$ abatement was only about 10%. Silver-alumina catalyst also exhibited good conversion of $NO_x$ in a narrow temperature range near 500ºC under simulated exhaust conditions with $O_2$ concentration in 1.5-10% range.[3] The performance of this catalyst rapidly deteriorates in the presence of $SO_2$ and $H_2O$.

In the last decade, several $NO_x$ removal technologies have been actively pursued and, at present, the urea selective catalytic reduction (SCR) system is the leading candidate for deployment. In order for large scale deployment of zeolite based catalysts for urea-SCR of diesel engine emission treatment, it is necessary to address several materials related issues. SCR catalyst performance gradually but persistently decreases under operating conditions and several mechanisms have been proposed including de-alumination, pore blockage, metal sintering, change of chemical states, acidity change, ammonia storage change, aging, and poisoning by Ca, P, Na, K, and S. A thorough understanding of the contribution of each of these pathways to ultimate failure of zeolite catalysts needs to be understood in order to design a catalyst system that can withstand the extreme environment of emissions. We will initiate our efforts by developing an understanding of failure modes that will enable us to synthesize new nano-catalyst systems. We will characterize these catalysts employing modern characterization tools and evaluate them on a bench-top reactor that simulates operating condition using simulated exhaust. The best catalysts will be aged under simulated operating conditions employing an accelerated aging protocol to determine its performance. The catalyst that meets all regulatory requirements in laboratory testing will be sent to John Deere for dynamometer testing. The criteria for a successful catalyst will include high temperature hydrothermal durability and a larger operating window for the zeolite catalyst.

## 1.2 PREVIOUS STUDIES

Zeolites play an important role in a variety of industries as catalysts (FAU-type), cement (natural zeolites), detergent (LTA-type), etc., and their use in membranes and sensors is under rapid development.[1] The successful applications of MFI- and CHA-type zeolites include their use as catalysts in Fluid Catalytic Cracking (FCC), propane upgrading,[2] and $NH_3$-Selective Catalytic Reduction (SCR) of $NO_x$ for engine emission aftertreatment.[3-5] The partial replacement of tetravalent silicon in zeolites with trivalent aluminum results in acidic sites which are responsible for catalytic activity.[6] The efforts to tailor catalytic performance of zeolites include cation exchange, morphology modification of cage size and channel shape[7] to increase the density of active acidic sites, and replacement of aluminum with boron (borosilicate)[8] or gallium (galliosilicate)[9] to tune the acidity of the active sites. Cation exchange generally leads to mononuclear centers for catalytic activity although a dinuclear metallic core, Cu-($\mu$-O)-Cu, has been reported by Solomon *et al*. as the effective catalytic site for $O_2$ activation.[10]

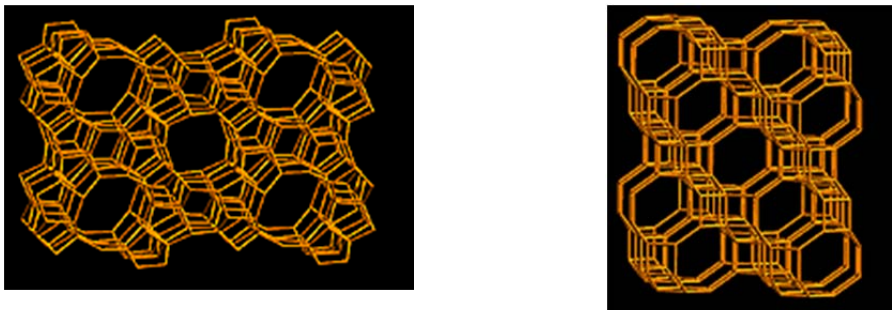

**Figure 1.1**. Left – MFI type zeolite frame-work of ZSM-5; Right Chabazite type framework of SSZ-13

The race to be compliant with regulatory requirements for diesel engine emissions (or high air-fuel ratio lean-burn gasoline engines) led to extensive work on zeolites and studies found Cu-ZSM-5[3,11,12] and Fe-ZSM-5[13-15] [Figure 1] to be highly effective $NH_3$-SCR catalysts for $NO_x$ reduction. The effective temperature range for Cu-ZSM-5 and Fe-ZSM-5 are 250 - 450°C and 350 - 650°C,[16,17] respectively, enabling a mixture of these two zeolites to reduce $NO_x$ in the 250 - 650°C range necessary for diesel engines to meet EPA Tier 4 emission standards for the United States. The persistent gradual loss in activity of Cu- and Fe-ZSM-5 led to a search for hydrothermally durable catalyst resulting in the discovery of Cu-SSZ-13[18-20] [Figure 1] as a $NH_3$-SCR catalyst which is now commercially available. Despite extensive efforts to improve the catalyst performance at low temperatures, including the use of alternative zeolites such as Cu-FAU[21] and Fe-Y[22], a catalyst that could effectively reduce $NO_x$ at 150ºC has remained elusive.

## 1.3 APPROACH

Since it is accepted that the first step in $NO_x$ conversion under SCR conditions involves NO oxidation to $NO_2$, we reasoned that catalyst modification that can enhance NO oxidation at low-temperatures should facilitate $NO_x$ reduction at low temperatures. Considering that Cu-ZSM-5 is a more efficient catalyst than Fe-ZSM-5 at low-temperature, we chose to modify Cu-ZSM-5. It is important to point out that the poor low-temperature efficiency of Fe-ZSM-5 has been shown to be due to selective absorption of $NH_3$ at low-temperatures rather than poor NO oxidation activity. In view of this, we also reasoned that an increased electron density on copper in Cu-ZSM-5 will inhibit any bonding with $NH_3$ at low-temperatures.

As stated earlier, the effective oxygen activation over a copper exchanged MFI zeolite,[10] whose active center, Cu-(μ-O)-Cu, closely resembles dinuclear metallic cores found in many important biological processes for small molecule activation, such as the Cu(μ-O)2Cu[23] core in "blue copper" for $O_2$ activation and the $Fe(\mu\text{-}O)_2Fe$[24] core in the MMO for methane activation, has been demonstrated. It can reasoned that a zeolite with a heterobimetallic dinuclear core, provided it can be synthesized, can be used to tailor catalytic activity of metal exchanged zeolite due to both enhanced redox power and increased spin flexibility.

If our reasoning is correct, we expected partial (or complete) replacement of aluminum with boron in Cu-ZSM-5 zeolites to result in a loss of $NO_x$ reduction activity because boron is more electronegative than aluminum and can reduce electron density at the copper sites. In addition, tetra-coordinate boron, bonded to four oxygen atoms, will not accommodate ammonia. We found that boron substitution indeed results in the loss of $NO_x$ reduction activity.

The partial (or complete) replacement of aluminum with iron in Cu-ZSM-5, on the other hand, should result in increased $NO_x$ reduciton activity. Indeed, we observed High $NO_x$ conversion by Cu-FeZSM-5 at low temperatures.

During our attempts to synthesize Cu-BZSM-5 and Cu-FeZSM-5, we discovered a new class of zeolites, heterobimetallic zeolites. We found that ion exchange does enable us to prepare heterobimetallic zeolites; however, the standard characterization tools do not enable the structure to be defined with certainty. **We report the exceptionally high catalytic activity of heterobimetallic zeolites for $NO_x$ reduction under $NH_3$-SCR conditions at low temperatures.**

## 2. CATALYST SYNTHESIS & TEST PROTOCOLS

### 2.1 SYNTHESIS

The samples of $Cu(OOCH_3)_2.H_2O$ were purchased from Sigma-Aldrich and that of $NH_4$-ZSM-5 (CBV-2314, $SiO_2/Al_2O_3$ = 23), $NH_4$-Zeolite-Beta (CP814E, $SiO_2/Al_2O_3$ = 25), and Na-Zeolite-Y (CBV-100, $SiO_2/Al_2O_3$ = 5) from Zeolyst International. All purchased precursors were used as received. The pyrolysis and calcination of $NH_4$-ZSM-5 and $NH_4$-Zeolite-Beta at 500°C (heating rate 10°C/min, hold 4 hours) furnished H-ZSM-5 and H-Beta, respectively. N,N,N-Trimethyladamantammonium Iodide[25] was prepared by a literature procedure for use as a template for the synthesis of H-SSZ-13[25,26].

The metal exchanged zeolites were prepared as follows:

**Cu-ZSM-5**: A 2.664 g sample of $Cu(OAc)_2 \cdot H_2O$ was dissolved in 600 mL de-ionized water (0.022M), followed by addition of H-ZSM-5 (10.00 g). The slurry was stirred for 2 hours at 50°C. The blue colored solid was collected by filtration after cooling, washed with de-ionized water, and calcined in air at 500°C (10°C/min) for 4 hours to obtain Cu-ZSM-5. Elemental analysis: Cu 2.76, Al 3.31%.

**Fe-ZSM-5**: H-ZSM5 (12.0 g) was suspended in a 600 mL degassed 0.02M $Fe(NO_3)_2$ water solution. The slurry was stirred for 24 hours at room temperature under $N_2$. A light pink solid was collected after filtration, dried at 100°C for 12 hours, and calcined in air at 550°C (5°C/min) for 4 hours to obtain Fe-ZSM-5 which was activated under a flow of He gas at 700°C for 1 hour. Elemental analysis: Fe 776 ppm.

**CuFe-ZSM-5**: 5 g Cu-ZSM-5 was suspended in a water solution of 25 mL 0.015M $Fe(NO_3)_3$, degassed with $N_2$, and kept stirring for 2 hours at 80°C. Brown solid was obtained after filtration, and the filtrate was clear and colorless. The product was then calcined in the air at 500°C (2°C/min) for 2 hours to yield pale yellow CuFe-ZSM-5. Elemental analysis: Cu 2.39, Fe 0.398, Al 2.97%

**CuFeN-ZSM-5** (N = 2, 4, 8, 20): The N in the formula refers to multiples of 25 ml of 0.015 M $Fe(NO_3)_3$ used in the ion exchange and not the ration of Cu to Fe. 5 g Cu-ZSM-5 was suspended in a water solution of 25 mL N x 0.015 M $Fe(NO_3)_3$, degassed with $N_2$, and kept stirring for 2 hours at 80°C. Brown solid was obtained after filtration, and the filtrate was red. The product was then calcined in the air at 500°C (2°C/min) for 2 hours to yield pale yellow CuFe-ZSM-5. Elemental Analyses: CuFe2-ZSM-5; Cu 1.7, Fe 0.51, Al 2.95%; CuFe4-ZSM-5; Cu 0.98, Fe 0.43, Al 2.91%; CuFe8-ZSM-5; Cu 0.61, Fe 0.28, Al 3.02%; CuFe20-ZSM-5; Cu 0.46, Fe 2.06, Al 3.04%;

**CuSc-ZSM-5**: 10 g Cu-ZSM-5 was suspended in a water solution of 50 mL 0.030M $Sc(NO_3)_3$, and was kept stirring for 2 hours at 80°C. Blue solid was obtained after filtration, and the filtrate was clear and colorless. The product was then calcined in the air at 500°C (2°C/min) for 2 hours to yield light blue CuSc2-ZSM-5. Elemental analysis: Cu 2.00, Sc 0.191, Al 2.94%

**CuIn-ZSM-5**: 10 g Cu-ZSM-5 was suspended in a water solution of 50 mL 0.015M $In(NO_3)_3$, and kept stirring for 2 hours at 80°C. Light blue solid was obtained after filtration, and the filtrate was clear and colorless. The product was then calcined in the air at 500°C (2°C/min) for 2 hours to yield light blue CuIn-ZSM-5. Elemental analysis: Cu 2.38, In 0.582, Al 2.91%

**CuLa-ZSM-5**: 10 g Cu-ZSM-5 was suspended in a water solution of 50 mL 0.015M $La(NO_3)_3$. The slurry was heated to 85°C for 2 hours, then cooled to room temperature, filtered, and washed

with deionized water to provide a blue solid. The blue solid was dried at 140°C (10°C/min) for 2 hours, and subsequently calcined at 500°C (10°C/min) for 2 hours with a heating rate of 10°C/min to yield CuLa-ZSM-5. Elemental analysis: Cu 2.96 , La 0.156, Al 3.28%

**Cu-Zeolite-Beta (Cu-Beta)**: A 2.664 g sample of $Cu(OAc)_2 \cdot H_2O$ was dissolved in 600 mL de-ionized water (0.022M), followed by addition of H-Beta (10.00 g). The slurry was stirred for 2 hours at 50°C. The blue colored solid was collected by filtration after cooling, washed with de-ionized water, and calcined in air at 500°C (10°C/min) for 4 hours to obtain Cu-Beta. Elemental analysis: Cu 2.54, Al 2.69%.

**CuFe-Zeolite-Beta (CuFe-Beta)**: 10 g Cu-Beta was suspended in a water solution of 50 mL 0.015M $Fe(NO_3)_3$, degassed with $N_2$, and kept stirring for 2 hours at 80°C. Yellow solid was obtained after filtration, and the filtrate was clear and colorless. The product was then calcined in the air at 500°C (2°C/min) for 2 hours to yield pale yellow CuFe-Beta. (Elemental analysis: Cu 1.74%; Fe 0.435%; Al 2.65%)

**Cu-SSZ-13**: A 2.664 g sample of $Cu(OAc)_2 \cdot H_2O$ was dissolved in 600 mL de-ionized water (0.022M), followed by addition of H-SSZ-13 (10.00 g). The slurry was stirred for 2 hours at 50°C. The blue colored solid was collected by filtration after cooling, washed with de-ionized water, and calcined in air at 500°C (10°C/min) for 4 hours to obtain Cu-SSZ-13. Elemental analysis: Cu 3.46, Al 4.05%.

**CuFe-SSZ-13**: 10 g Cu-SSZ-13 was suspended in a water solution of 50 mL 0.015M $Fe(NO_3)_3$, degassed with $N_2$, and kept stirring for 2 hours at 80°C. Yellow solid was obtained after filtration, and the filtrate was clear and colorless. The product was then calcined in the air at 500°C (2°C/min) for 2 hours to yield pale yellow CuFe-SSZ-13. Elemental analysis: Cu 2.71, Fe 0.357, Al 3.86%

**H-[B]ZSM-5**[27]: In a plastic bottle, 10.024 g $NH_4$-ZSM-5 was stirred in a 500 mL 0.2 M $NH_4BF_4$ solution buffered to pH = 7.3 with $NH_4OAc$. The mixture was heated at 85°C for 18 hours. The obtained powder after filtration and wash was further exchanged with a solution of $NH_4NO_3$ (2M, 200 mL) at 80°C for 3 hours. White powder was obtained after filtration, wash, and calcinations at 500°C (10°/min) for 4 hours. Elemental analysis shows B 266 ppm.

**Cu-[B]ZSM-5**: 0.532 g $Cu(OAc)_2 \bullet H_2O$ was dissolved in 80 mL de-ionized water, followed by addition of 2.00 g H-[B]ZSM-5. The slurry was kept stirring for 4 hours at 50°C. Blue solids were collected by filtration after cooling, washed with de-ionized water, and calcined in air at 500°C (10°C/min) for 4 hours. Elemental analysis shows Cu 2.79% and B 52 ppm.

**BZSM-5**: A 1.092 g sample of $B(OH)_3$ was dissolved in a 111 mL solution containing 21.180 g $NPr_4OH$. The solution was kept stirring for 30 minutes, followed by addition of 12.2 g silicic acid. The gel formed was stirred for another hour and transferred to a Parr autoclave, and heated at 150°C for 5 days, cooled to room temperature, filtered, washed with de-ionized water, and calcined at 650°C (5°/min) for 2 hours to provide a white powder. H-BZSM-5 was synthesized as following: a 6.0 g sample of BZSM-5 was exchanged with 600 mL 1.0 M $NH_4OAc$ solution at 80°C for 12 hours. The powder was isolated by filtration, washed, dried, and calcined at 500°C (10°/min) for 4 hours.

**Cu-BZSM-5**: 3.787 g $Cu(OAc)_2 \bullet H_2O$ was dissolved in 800 mL de-ionized water, followed by addition of 14.081 g H-BZSM-5. The slurry was kept stirring for 4 hours at 50°C. Pale green solids were collected by filtration after cooling, washed with de-ionized water, and calcined in air at 500°C (10°C/min) for 4 hours. Elemental analysis shows Cu 1.58%.

**Cu-[FeZSM-5]:** The synthesis of Cu-[FeZSM-5]51 requires multiple steps. First, [FeZSM-5]51 samples were prepared according to a literature procedure (J. Chem. Soc., Farraday Trans. 1,

**1987**, *83*, 487-494) starting with 3.75 g $Fe(NO_3)_3 \cdot 9H_2O$ and 50.0 g N-brand silica. A 13.0 g sample of [FeZSM-5]51 was exchanged with 800 mL $NH_4NO_3$ (1.0 M aqueous solution) at 80°C for 12 hours, filtered, washed, and calcined at 500°C (10°C/min) for 4 hours to obtain light yellow powder 11.4 g of H-[FeZSM-5]51.

**Cu-[FeZSM-5]51:** 6 g H-[FeZSM-5]51 was suspended in a $Cu(OAc)_2$ solution (1.597 g $Cu(OAc)_2 \cdot H_2O$ in 360 mL deionized water). The mixture was heated to 50°C for 2 hours. Light green/yellow powder was obtained after filtering, washing and calcining at 500°C (10°C/min) for 2 hours. Elemental Analysis: Cu 1.44%; Fe 3.10%; Si 41.0%; $SiO_2/Fe_2O_3$ = 53; Cu exchange degree 82%.

The synthesis of Cu-[FeZSM-5]23 also requires multiple steps. After mixing 15 g $Fe(NO_3)_3 \cdot 9H_2O$, 100 g N-brand silica, and other necessary reagent in the right order, no gel formation was observed. The solution was yellow and clear with a pH less than 1. NaOH solution with appropriate concentration was titrated into the above acidic solution till the pH of the reaction mixture increased to pH ~ 10 resulting in a yellow gel formaton. Tetrapropylammonium bromide was added to the yellow gel, and a pale [FeZSM-5]23 powder (35 g) was obtained after hydrothermal synthesis. 23 g of [FeZSM-5]23 powder was first exchanged with 1.6 L $NH_4NO_3$ (1 M) at 80°C for 12 hours, then filtered, washed, and calcined at 500°C (10°C/min) for 4 hours to obtain light yellow powder of H-[FeZSM-5]23.

**Cu-[FeZSM-5]23.** 10 g H-[FeZSM-5]23 was suspended in a $Cu(OAc)_2$ solution (2.662 g $Cu(OAc)_2 \cdot H_2O$ in 600 mL deionized water). The mixture was heated to 50°C for 2 hours. Yellow powder (9.9 g) was obtained after filtering, washing and calcining at 500°C (10°C/min) for 2 hours. Elemental Analysis: Cu 1.96%; Fe 5.79%; Si 38.5%; $SiO_2/Fe_2O_3$ = 26; Cu exchange degree 60%. The Cu-[FeZSM-5]23 has comparable Cu loading and physical appearance as observed in CuFe-ZSM-5 obtained from Cu-ZSM-5. Interestingly, the higher Si/Fe ratio catalyst Cu-[FeZSM-5]51 shows higher degree of Cu exchange and slightly different color in green/yellow.

## 2.2 DEGREENING AND $NO_X$ CONVERSION EFFICIENCY

The protocols for degreening, testing, and aging of off-road engine catalysts have been provided to us by our collaborators at John Deere Power Systems.

The catalyst powders were mixed with an equal amount (by weight) of inert cordierite and transferred to a bench-top reactor (Scheme S1). A degreening was done in a flow of 8.5% $O_2$, 8% $CO_2$, and 7.25% $H_2O$ with balance $N_2$ at 600°C (inlet gas temperature) and a space velocity of 50,000 $h^{-1}$ for two hours. $NO_x$ conversion efficiency experiments employed simulated diesel exhaust containing 8.5% $O_2$, 8% $CO_2$, 7.25% $H_2O$, 250 ppm $NO_2$, 250 ppm NO, 500 ppm $NH_3$, and $N_2$ as balance at a space velocity of 50,000 $h^{-1}$ and evaluated in the 150-650°C temperature range.

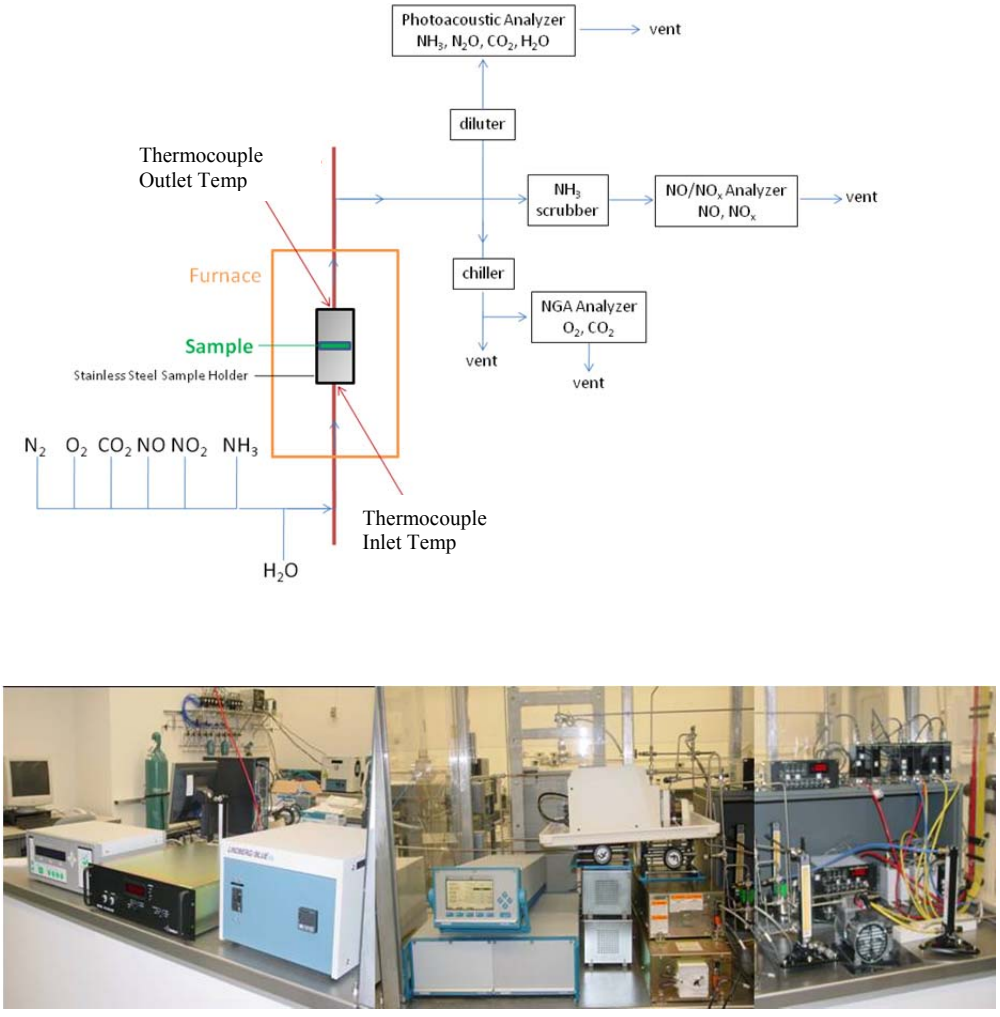


**Figure 2.1.** Schematics and picture of the bench-top reactor fitted with Innova 1314 gas analyzer (California Analytical Instruments, Inc.) monitored $NH_3$, $CO_2$, $N_2O$, and $H_2O$, a chemiluminescence 600 HCLD analyzer (California Analytical Instruments, Inc.) monitored $NO/NO_x$, and $O_2$ was monitored by a Rosemount NGA 2000 Multi-Component gas analyzer using a paramagnetic oxygen sensor.

## 2.3 AGING PROTOCOL

The aging protocol involves exposing catalysts to a flow of $O_2$, $H_2O$ and $N_2$ balance at a space velocity of 10,000 $hr^{-1}$ for 50 hours at 675°C.

## 3. CATALYST CHARACTERIZATION

The structural characterization of heterobimetallic zeolites with UV-Vis, EPR, XRD, and EXAFS did enable us to define the structure to certain extent. It can be reasoned that an ion exchange of monometallic zeolite can result in (1) the deposition of metal oxide particles on the zeolite surface; (2) exchange of zeolite metal with heteroatom to produce a mixture of heteroatom zeolite with parent zeolite; (3) replacement of framework Al with heteroatom; (4) partial replacement of zeolite metal with heteroatom at dinuclear sites to form M-O-M' sites; or (5) incorporation of heteroatom metal oxide clusters linked to the active metal centers in the zeolites' straight channel. The results of characterization studies, described in the following paragraphs, enable us to rule out surface deposition and formation of a mixture of heteroatom zeolite with parent zeolite.

### 3.1 ZSM-5 TYPE HETEROBIMETALLIC ZEOLITES

The X-ray powder diffraction pattern of CuFe-ZSM-5 exhibits a typical MFI-zeolite diffraction pattern suggesting that $Fe^{3+}$ incorporation in Cu-ZSM-5 did not result in phase change or structural distortion (Figure 3.1).

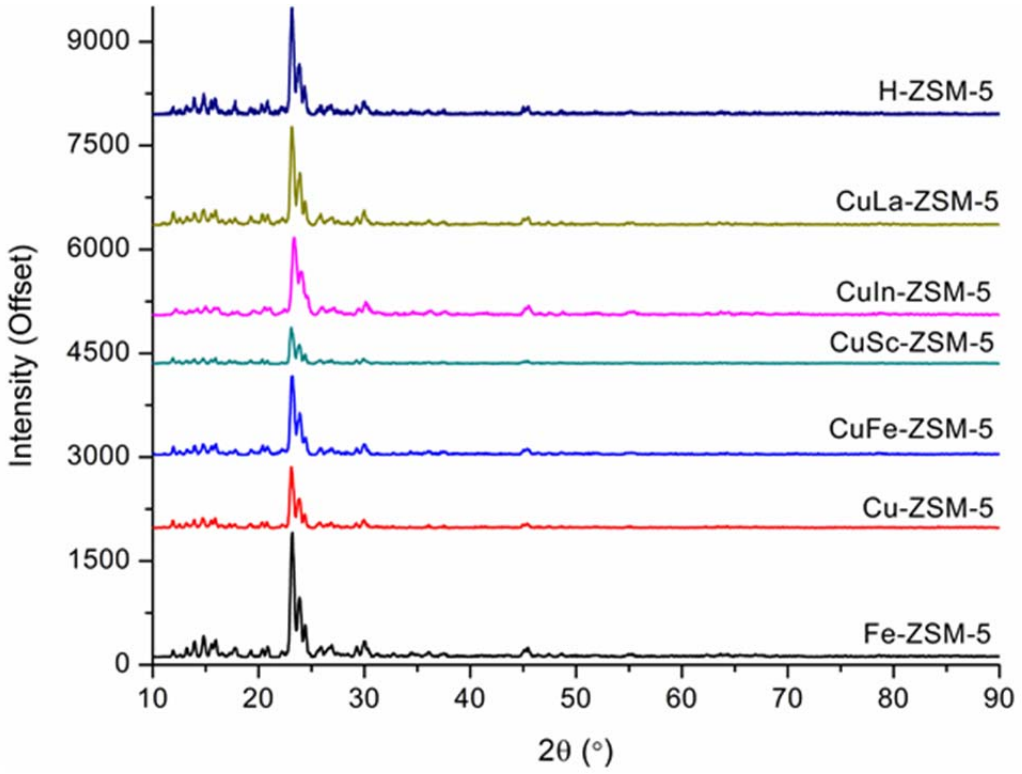


**Figure 3.1.** Powder XRD of ZSM-5 based catalyst.

The UV-Vis spectrum of (Figure 3.2A) CuFe-ZSM-5 exhibits typical features of Cu-ZSM-5, which include a very intense absorption from d-d transitions at ~200 nm and a broad peak at ~830 nm (Figure 3.2A, inset) from the charge transfer band related to O→Cu transition from lattice oxygen to isolated $Cu^{2+}$ ions.[28] In addition, CuFe-ZSM-5 has two absorptions that can be attributed to framework tetrahedral and extra-framework octahedral $Fe^{3+}$, at 210 nm and 270 nm, respectively, as seen in Fe-ZSM-5 type structures.[15] In general, absorptions of oligomeric iron oxide clusters and iron oxide particles are believed to be above 400 nm[15] and are not seen. A new, intense absorption centered at ~350 nm (Figure 3.2A) is also present. This unique absorption may be attributed to d-d transitions promoted by the interaction of copper and iron, i.e., transitions from half occupied d orbitals of $Fe^{3+}$ to the only empty $d_{eg*}$ orbital of $Cu^{2+}$.

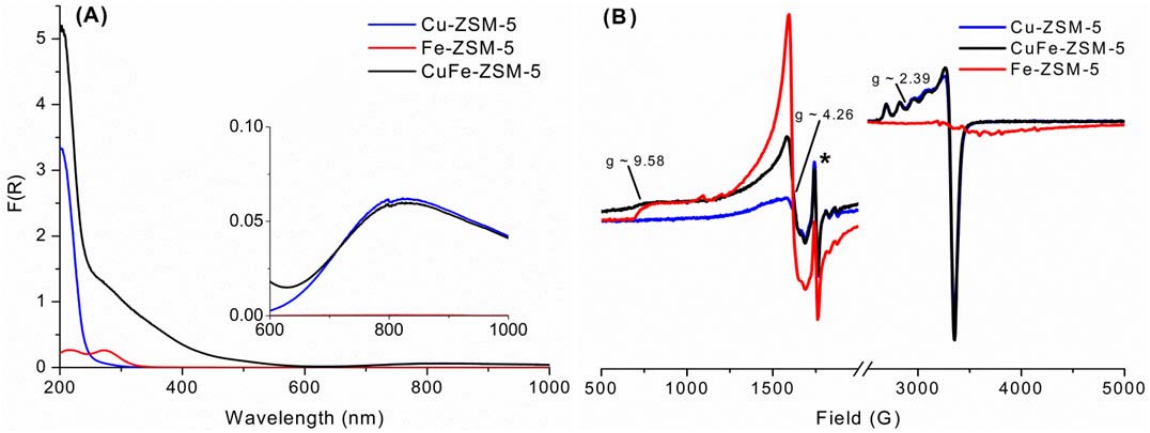


**Figure 3.2.** Diffuse reflectance UV-Vis (A) and EPR (B) of Cu-ZSM-5, Fe-ZSM-5, and CuFe-ZSM-5. (The star marked EPR signals are verified to originate from the resonator).

The EPR spectrums of Cu-ZSM-5 and Fe-ZSM-5 resemble those reported in literature (Figure 3.2B).[15,28] The EPR of CuFe-ZSM-5 (Figure 3.2B) is similar to that of Cu-ZSM-5 with a signal at g ~ 2.4 and resolved fine hyperfine-coupling, consistent with the experimentally observed square planar geometry.[29-31] The higher EPR intensity of the signal at g ~ 4.3 of CuFe-ZSM-5 as compared with the signal in Cu-ZSM-5 suggests tetrahedral $Fe^{3+}$, generally observed in EPR of Fe-ZSM-5,[15] supports the presence $Fe^{3+}$ incorporation in CuFe-ZSM-5. EXAFS studies of the CuFe-ZSM-5 sample, however, did not allow us to discern the presence of metals heavier than $Al^{3+}$ near the discrete $Cu^{2+}$ active center with a square planar geometry (Figure 3.3).

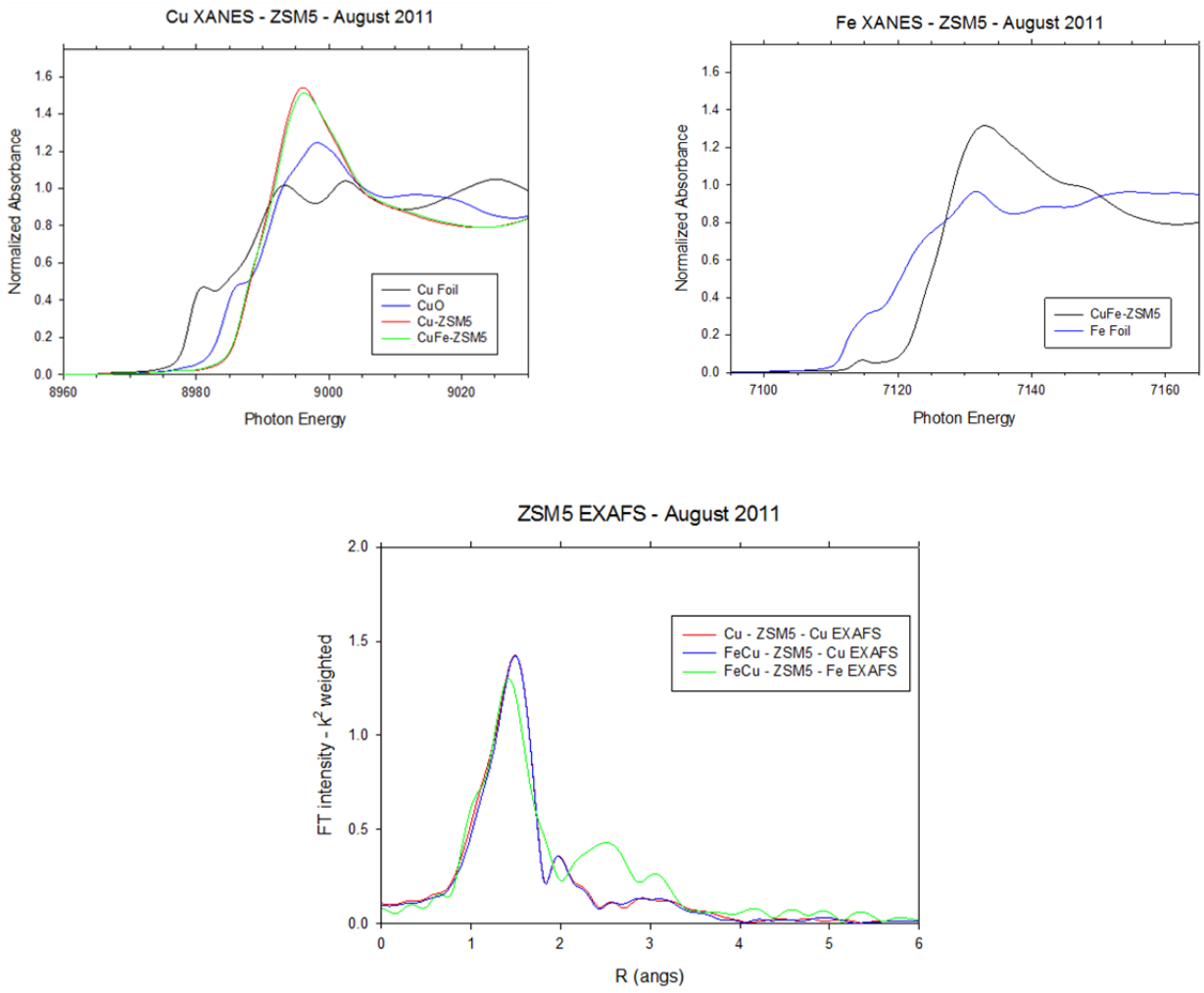


**Figure 3.3:** XANES and EXAFS of Cu-ZSM-5 and CuFe-ZSM-5

## 3.2 SSZ-13 TYPE HETEROBIMETALLIC ZEOLITES

The X-ray powder diffraction pattern of CuFe-SSZ-13 exhibits a typical CHA-zeolite diffraction pattern suggesting that $Fe^{3+}$ incorporation in Cu-SSZ-13 did not result in phase change or structural distortion (Figure 3.4).

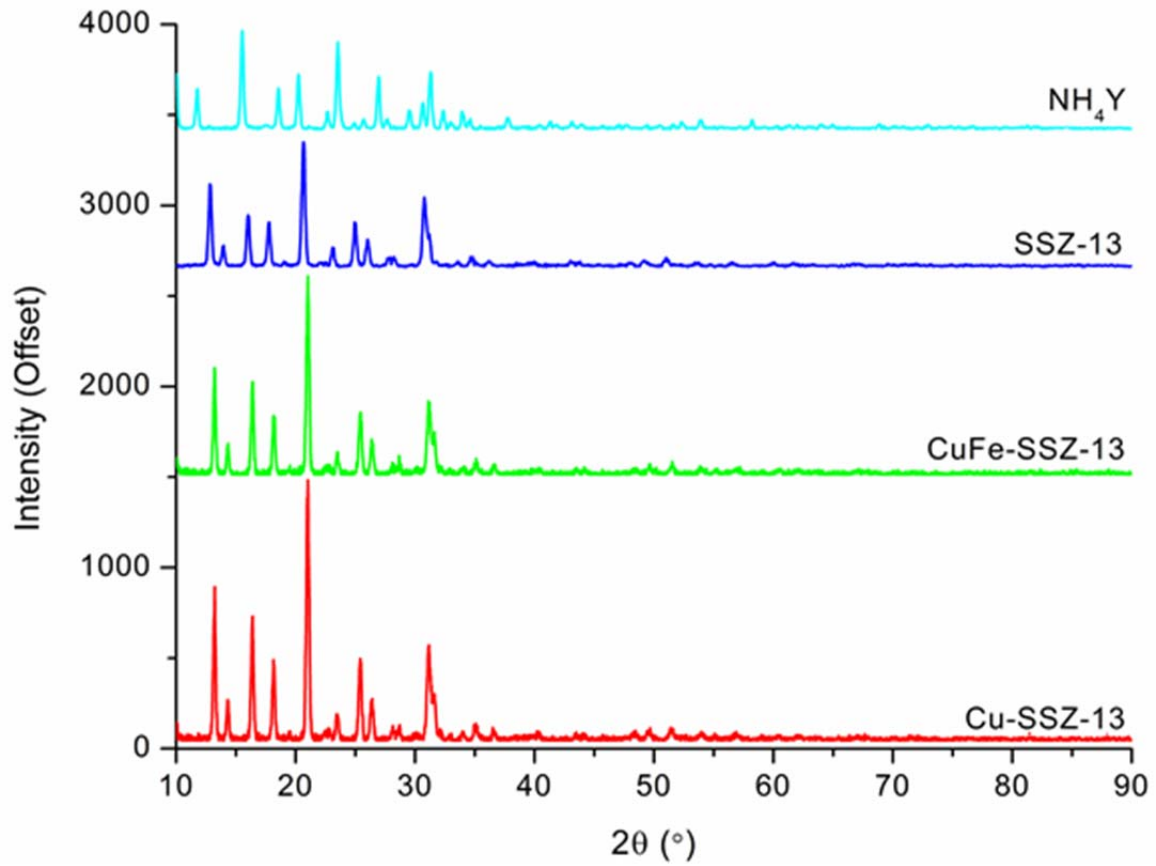


**Figure 3.4:** Powder XRD of zeolite Y, SSZ-13, Cu-SSZ-13 and CuFe-SSZ-13.

## 4. $NO_X$ CONVERSION EFFICIENCY OF CATALYSTS

The extensive research on Cu-ZSM-5 and Fe-ZSM-5 as $NO_x$ reduction catalysts for diesel engines operating in the transportation sector provided us with the impetus to test these zeolites for their ability to treat $NO_x$ emissions from off-road diesel engines (i.e. engines operating in heavy machinery, agricultural equipment etc.).[1-6] Since the off-road diesel engine emissions constituent ratios are close to the ones needed for "fast SCR", we expected high $NO_x$ conversion efficiency from these catalysts. Our results are shown in Figure 4.1. Cu-ZSM-5 exhibits a 90% $NO_x$ reduction efficiency in 250-400°C range with a rapid reduction to ~60% in 450-650°C. Fe-ZSM-5, on the other hand, efficiently reduces $NO_x$ (> 90%) in the 350-550°C range. Thus, a combination of Cu-ZSM-5 and Fe-ZSM-5 can be expected to reduce $NO_x$ efficiently in the 250-650°C range. However, both catalysts are able to convert only 30% of the $NO_x$ at 150°C, although, the $NO_x$ conversion efficiency increase rapidly over the 150-250°C range.

.

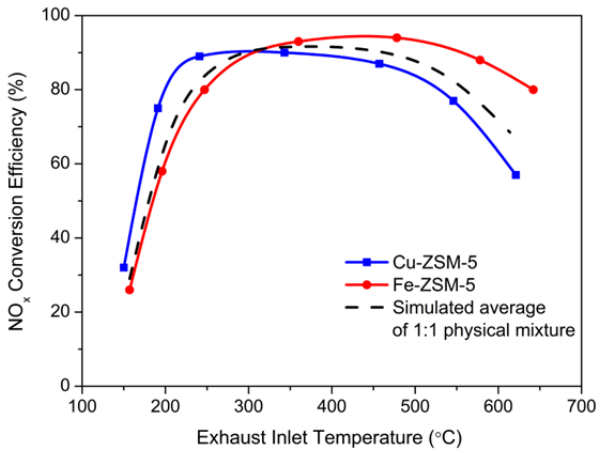


**Figure 4.1**. $NO_x$ conversion efficiency of Cu-ZSM-5 and Fe-ZSM-5 tested with simulated off-road diesel engine exhaust. The performance of a physical mixture (1:1) of Cu-ZSM-5 and Fe-ZSM-5 is simulated as an average of the tested results from the two catalysts in black dashed line.

We expected partial (or complete) replacement of aluminum with boron in Cu-ZSM-5 zeolites to result in a loss of $NO_x$ reduction activity because boron is more electronegative than aluminum and can reduce electron density at copper sites. In addition, tetra-coordinate boron, bonded to four oxygen atoms, will not accommodate ammonia. The iron substitution, on the other hand, was expected to enhance $NO_x$ reduction. The results, to some extent, confirmed our expectations but led to discovery of a new class of heterobimetallic zeolites. Our results are presented in the following sections.

### 4.1 BORON SUBSTITUTED Cu-ZSM-5

Partial substitution of boron in Cu-ZSM-5 proved quite difficult. The partial replacement of aluminum, employing ammonium tetrafluoroborate, resulted in incorporation of 260 ppm of boron.[27] A significant portion of this boron was lost on treatment with $Cu(OAc)_2$ during our attempts to synthesize Cu-B-ZSM-5 (52 ppm found in Cu-[B]ZSM-5). The treatment of Cu-

ZSM-5 with ammonium tetrafluoroborate did not lead to Cu-B-ZSM-5 but resulted in a loss of $Cu^{2+}$, probably due to high concentration of $OAc^-$ necessary for the isomorphous boron substitution. The failed attempts to obtain partial substitution of aluminum with boron in Cu-ZSM-5 led us to employ H-BZSM-5 which can be directly synthesized. A standard solution exchange $Cu(OAc)_2$ furnished Cu-BZSM-5 as a light green powder. Elemental analysis shows a Cu content at 1.58% which is about 2/3 of copper content in Cu-ZSM-5.

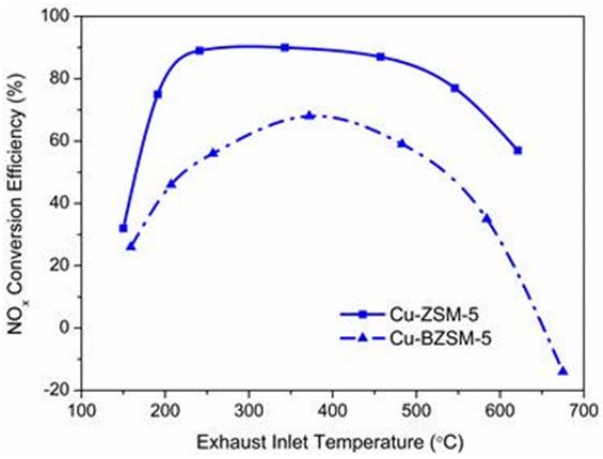


**Figure 4.2**. $NO_x$ conversion on Cu-BZSM-5 vs. Cu-ZSM-5 (right)

As expected, the NOx conversion efficiency of Cu-BZSM-5 (Figure 4.2) is significantly lower than Cu-ZSM-5 at all temperatures. After a single test run, the light green Cu-BZSM-5 powder turned to brown, indicating changes in the $Cu^{2+}$ cation location and speciation. The copper ions might have migrated to extra framework positions or in the pores or the channels as copper oxides at high temperatures

## 4.2. IRON SUBSTITUTED Cu-ZSM-5

A comparison of $NO_x$ conversion over Cu-ZSM-5, CuFe-ZSM-5, and Cu-[FeZSM-5]51under off-road diesel engine ammonia-SCR conditions is shown in Figure 4.3. With only $Fe^{3+}$ at the tetrahedral supporting position other than the $Al^{3+}$, Cu-[FeZSM-5]51 doubles the $NO_x$ conversion efficiency as compared to Cu-ZSM-5 at 150°C, and perfectly matches the $NO_x$ reduction performance as that of the CuFe-ZSM-5 at low temperature range (150°C-250°C). This strongly supports our proposal that iron in CuFe-ZSM-5 introduced via ion exchange in Cu-ZSM-5 occupies framework location. This means that the Cu-O-Fe unit, formed from partial $Fe^{3+}$ substitution of the supporting tetrahedral $Al^{3+}$ in CuFe-ZSM-5, is responsible for the low temperature $NO_x$ conversion enhancement as compared with that of Cu-ZSM-5. The significant loss of higher temperature efficiency from Cu-[FeZSM-5]51 may be attributed to the low population of $Fe^{3+}$ at the octahedral position.

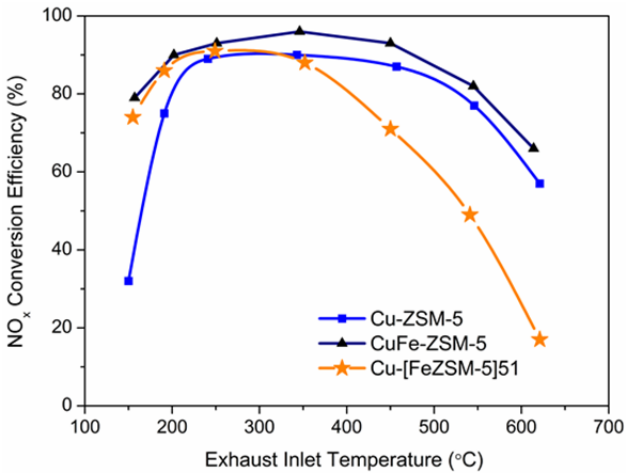


**Figure 4.3.** Ammonia-SCR $NO_x$ conversion over Cu-ZSM-5, CuFe-ZSM-5, and Cu-[FeZSM-5]51.

## 4.3 HETEROBIMETALLIC ZEOLITES

The CuFe-ZSM-5 powder exhibits an 80% $NO_x$ conversion efficiency at 150°C (Figure 4.4a) and maintains a ~ 90% conversion efficiency in the 200-450°C range which drops to 68% at 650°C. To our knowledge, the CuFe-ZSM-5 is the first catalyst that can effectively reduce $NO_x$ at 150°C at 50k $h^{-1}$ space velocity. In comparison, the Cu-ZSM-5 powder shows only 30% $NO_x$ conversion at 150°C which gradually increases to 90% at 250°C but starts to drop below 90% at 450°C and 58% at 625°C. The Fe-ZSM-5 powder exhibits 90% $NO_x$ conversion efficiency in the 350-550°C range which drops to ~ 80% at 650°C. The $N_2O$ production (Figure 4.4B) during SCR with CuFe-ZSM-5 reaches maximum at 150°C and then is identical to that of Cu-ZSM-5 in the 200-650°C range. Fe-ZSM-5 does not produce $N_2O$ at all during the SCR catalytic cycle. Thus, the low temperature reactivity of CuFe-ZSM-5 can be attributed to a synergistic effect resulting from the incorporation of $Fe^{3+}$ in close proximity to $Cu^{2+}$. Combining the results of catalytic behavior with the results of XRD, UV-VIS, EXAFS, and EPR studies of CuFe-ZSM-5 enable us to rule out surface deposition and formation of Cu-ZSM-5 and Fe-ZSM-5 mixture as description of the CuFe-ZSM-5 structural properties.

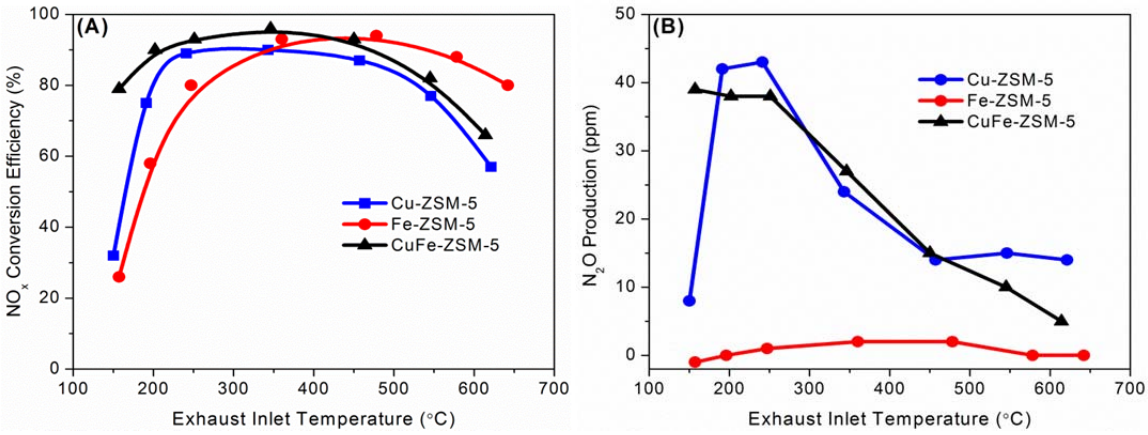


**Figure 4.4.** $NO_x$ conversion efficiency (A) and $N_2O$ production (B) patterns of CuFe-ZSM5 compared to that of Cu-ZSM5 and Fe-ZSM5 tested with simulated off-road diesel engine exhaust.

All three catalysts exhibit typical fast SCR behaviors, i.e., correlated consumption of $NH_3$ and $NO_x$ in ~ 1:1 ratio up to 400°C (Figure 4.5). The $N_2$ formation selectivity (Figure 4.6 left) of CuFe-ZSM-5 is similar to that of Cu-ZSM5. It is important to note that no $NO_x$ reduction is observed in the absence of ammonia, suggesting that CuFe-ZSM-5 is not effective as a $NO_x$ reduction catalyst under oxidizing environment of diesel engine emissions (Figure 4.6 right).

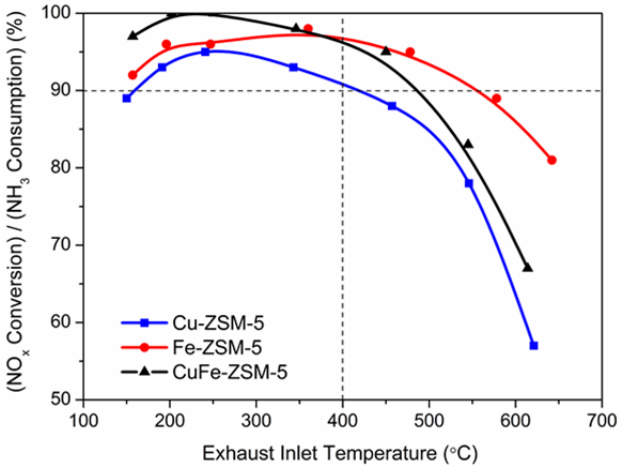


**Figure 4.5.** $NO_x$ conversion efficiency vs. $NH_3$ consumption ratio with a cutoff value set at 90% to track the "Fast SCR Reaction": $2NH_3 + NO_2 + NO \rightarrow N_2 + H_2O$

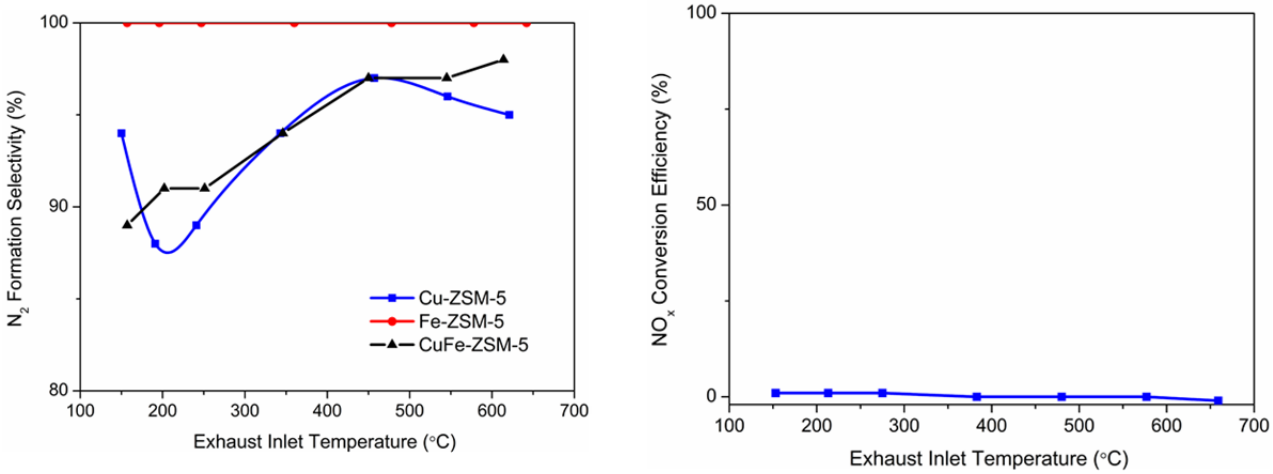


**Figure 4.6:** $N_2$ formation selectivity, defined as (reduced_$NO_x$ – $N_2O$_production)/ reduced_$NO_x$, of catalyst Cu-ZSM-5, Fe-ZSM-5, and CuFe-ZSM-5 (Left). $NO_x$ conversion in the absence of $NH_3$ over CuFe-ZSM-5 under the following condition: 8.5% $O_2$; 8% $CO_2$; 7.25% $H_2O$; 250 ppm NO; 250 ppm $NO_2$ with $N_2$ as balance (Right)

## 4.3 GENERALITY OF ION EXCAHNGE FOR SYNTHESIS OF HETEROBIMETALLIC ZEOLITES

The successful incorporation of $Fe^{3+}$ into Cu-ZSM-5 (i.e. CuFe-ZSM-5), resulting in enhanced low temperature $NO_x$ reduction efficiency, prompted us to explore the generality of the method for synthesis of other heterobimetallic zeolites. We selected $Sc^{3+}$, $In^{3+}$, and $La^{3+}$ based on their preferred 3+ oxidation states under oxidizing environment. Furthermore, these elements represent different electronic configurations. $Sc^{3+}$ has no d electrons with five empty d orbitals enabling it to interact with $Cu^{2+}$ via bridging oxo atoms or direct metal-metal interaction; all of the $In^{3+}$ d orbitals are fully occupied preventing direct metal-metal interaction with $Cu^{2+}$ centers; $La^{3+}$ can interact with $Cu^{2+}$ via d-f exchange.[33] Thus, one can expect varying catalytic activity due to varying electronic influence over the $Cu^{2+}$ center.

The degree of heteroatom incorporation in Cu-ZSM-5 varies among these elements, and the incorporation of $In^{3+}$, $Sc^{3+}$, and $La^{3+}$ decreases with the increase in ionic radius of these heteroatoms. All new catalysts exhibit the same ZSM-5 powder diffraction pattern (Figure S1). Subtle changes are observed in the $NH_3$ TPD spectra (Figure S9) of these catalysts that may be a result of the small dosage of the trivalent element or increased hindrance for $NH_3$ interaction due to heteroatom incorporation. As expected (Figure S10), the UV-Vis of CuSc-ZSM-5 and CuLa-ZSM-5 are essentially identical to that of Cu-ZSM-5. CuIn-ZSM-5 is also identical to Cu-ZSM-5 except it exhibits an additional absorptions ~ 300 nm due to d-d transitions. It is important to note that nanoscale $In_2O_3$ also exhibits strong absorption around 300 nm.[34,35]

All new heterobimetallic MFI-zeolite catalysts, CuM-ZSM-5, consistently exhibit >70% $NO_x$ conversion efficiency at 150°C, maintain a ~ 90% conversion efficiency in 200-450°C range, and

exhibit a drop to ~ 60% above 600°C (Figure 4.7). Lanthanide containing CuLa-ZSM-5 has the best low temperature performance but its efficiency also has the fastest drop after 500°C.

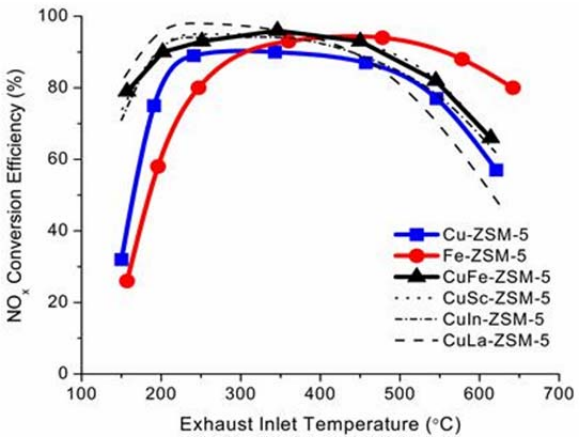


**Figure 4.7.** $NO_x$ conversion efficiency of CuM-ZSM-5 (M = Sc, Fe, In, and La) compared to that of Cu-ZSM5 and Fe-ZSM5 tested with simulated off-road diesel engine exhaust.

## 4.4 EFFECTS OF ZEOLITE FRAMEWORK

The examples presented in the preceding section show that it is possible to incorporate a variety of heteroatoms in ZSM-5 structures. This section explores the effect of heteroatom incorporation on catalytic activity of metal exchanged zeolite with framework other than ZSM-5. We selected Cu-Beta [BEA] and Cu-SSZ-13 [CHA], which have also been explored as SCR catalysts,[18-20] to gain insights in framework effects. A Cu-Beta with a Si/Al ratio similar to that of the Cu-ZSM-5 employed in this study was used and the ion exchange approach was used to prepare Cu-Beta and CuFe-Beta. Cu-SSZ-13 and CuFe-SSZ-13 were also synthesized by the step-wise ion exchange.

The framework structure of zeolite Beta remains intact after the sequential solution exchange with $Cu^{2+}$ and $Fe^{3+}$ as indicated by the XRD powder diffraction pattern. The UV-Vis spectra of Cu-Beta and CuFe-Beta resemble those of Cu-ZSM-5 and CuFe-ZSM-5, respectively. The charge transfer band O→Cu near 800 nm is present in both Cu-Beta and CuFe-Beta. In addition to all of the absorptions of Cu-Beta, CuFe-Beta also exhibits three extra absorptions at 270, 360, and 500 nm which are assigned to extra-framework octahedral $Fe^{3+}$, Cu/Fe units with bridging oxo(s), and iron oxides, respectively. The presence of iron in CuFe-Beta does not result in enhanced $NO_x$ conversion efficiency (Figure 4.8A) when compared to Cu-Beta at 150°C. Between 200°C and 250°C, CuFe-Beta shows identical $NO_x$ reduction efficiency as Cu-Beta, and both are comparable with CuFe-ZSM-5. Above 250°C, CuFe-Beta gradually loses its $NO_x$ conversion capability, while Cu-Beta maintains a $NO_x$ conversion curve parallel to but slightly below that of CuFe-ZSM-5. It is probable that the lack of a square planar coordination environment in zeolite beta, identified to be the preferred Cu binding site in ZSM-5, hampers the effective function of the heterometallic Cu/Fe core to boost the low temperature $NO_x$ conversion efficiency.

CuFe-SSZ-13 exhibits high $NO_x$ reduction efficiency at low temperature reminiscent of CuFe-ZSM-5 (Figure 4.8B). In addition, the greenhouse gas $N_2O$ production from CuFe-SSZ-13 is 50% less than that from CuFe-ZSM-5 at the peak value. This result can be attributed to the unique framework of SSZ-13, which also possesses suitable locations of perfect square planar coordination environments to host $Cu^{2+}$ and the sites for Cu/Fe linkage.

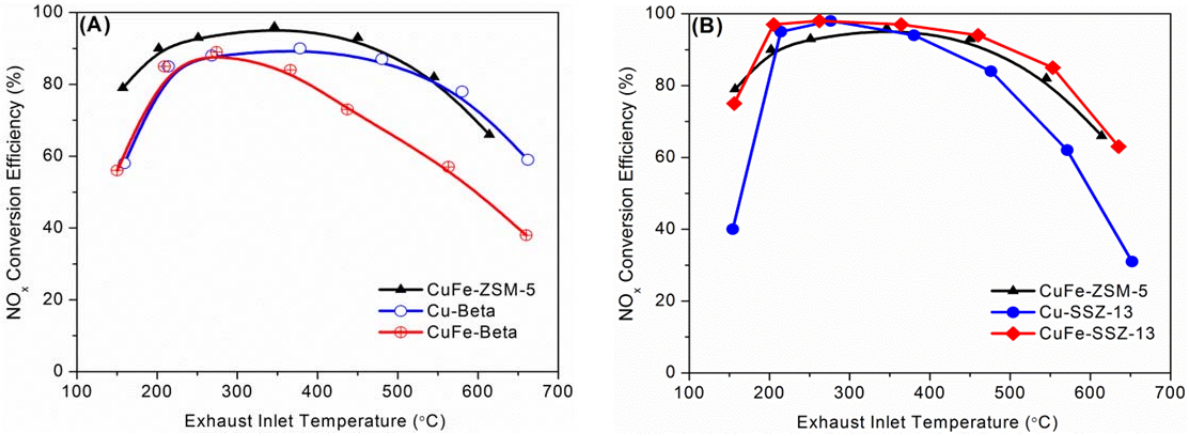


**Figure 4.8.** $NO_x$ conversion efficiency of (A): CuFe-ZSM-5, Cu-Beta, and CuFe-Beta; (B) CuFe-ZSM-5, Cu-SSZ-13, and CuFe-SSZ-13.

## 4.5 IMPACT OF $NO_2$:$NO_x$ RATIO

For this experiment, CuFe-SSZ-13 was loaded on a honeycomb employing dilute silica sol with a loading of 30% w/w catalyst. The results show the impact $NO_2/NO_x$ ratio on $NO_x$ conversion efficiency at temperatures below 200ºC (Figure 4.9). At ~150ºC and $NO_2/NO_x$ ratio of 0.5, the $NO_x$ conversion efficiency is ~70%. Reducing $NO_2$ leads to reduced $NO_x$ conversion and ZERO $NO_2$ results in $NO_x$ conversion of ~40%. Increasing temperature to 195°C eliminates the impact of $NO_2$/NO ratio and $NO_x$ conversion is <95%.

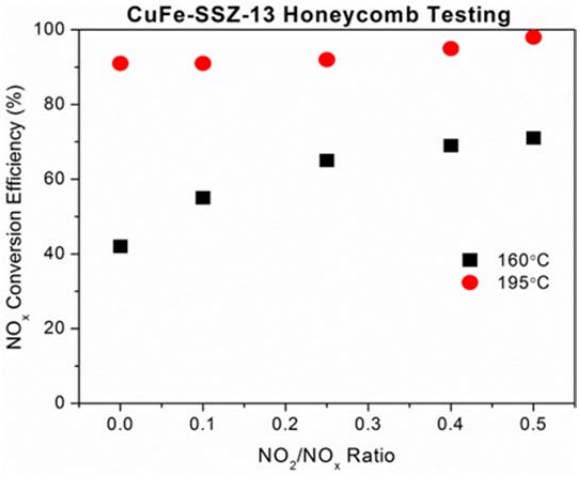


**Figure 4.9:** $NO_x$ conversion efficiency of CuFe-SSZ-13 at 160ºC and 195ºC as a function of $NO_2/NO_x$ ratio

## 4.5 HYDROTHERMAL STABILITY

We carried out accelerated testing by employing an aging protocol that exposes catalyst to 675°C for 50 hours under a flow of air containing 10% water. The zeolite catalysts are well-known to deteriorate gradually via dealumination under emission treatment conditions resulting in the loss of catalyst sites.[36-38]The X-ray powder diffraction patterns of all catalysts, described in this study, show that zeolite framework is retained after accelerated aging, but the aging does result in the partial loss of $NO_x$ reduction performance (Figure 4.10). Fe-ZSM-5 shows at least 20 percent loss of $NO_x$ conversion activity over the entire testing temperature range. Cu-ZSM-5 retains ~80% $NO_x$ conversion between 250°C and 450°C. The observed efficiency loss of Cu-ZSM-5 and Fe-ZSM-5 is consistent with the loss of efficiency observed upon subjecting these zeolites to accelerated aging under on-road diesel engine conditions.[36,39,40] The introduction of heteroatom in ZSM-5 structure neither enhances nor reduces hydrothermal stability of MFI zeolites. The hydrothermal stability of CuM-ZSM-5 resembles that of Cu-ZSM-5.

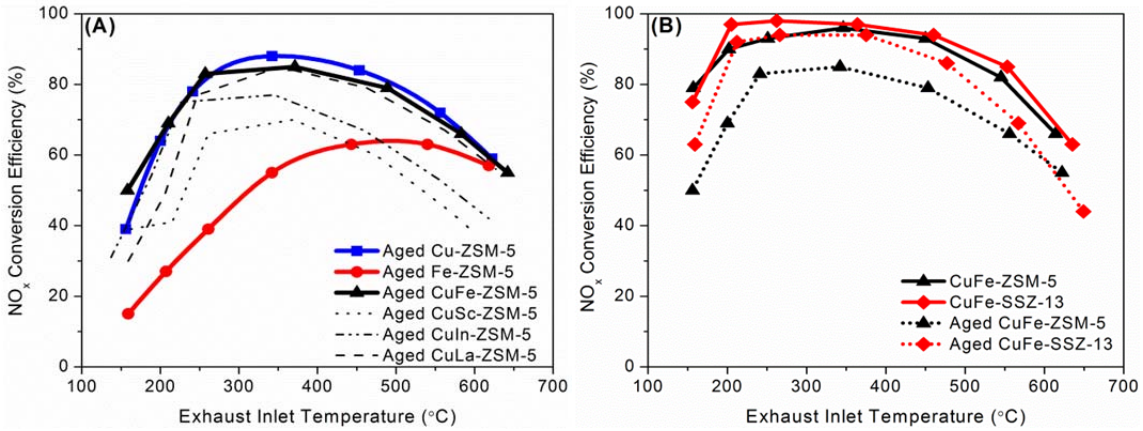


**Figure 4.10.** $NO_x$ SCR comparison of Cu-ZSM-5, Fe-ZSM-5, and CuFe-ZSM-5 after hydrothermal aging.

The chabazites [CHA], on the other hand, exhibit remarkably hydrothermal durability. The activity of Cu-SSZ-13 is not adversely impacted by incorporation of iron. Interestingly, the low temperature activity of CuFe-SSZ-13 experiences moderate drop occurs at 150°C but negligible change in 200-450°C range (Figure 4.10B). Thus, CuFe-SSZ-13 is an ideal catalyst for $NO_x$ conversion performance in 150-650°C range and is hydrothermal stable.

## 5. MECHANISTIC STUDIES

As mentioned earlier, the standard characterization and $NO_x$ conversion activity experiments ruled out the deposition of iron oxide on Cu-ZSM-5 surface and exchange of Cu with iron to produce a mixture of Cu-ZSM-5 and Fe-ZSM-5 as possible results of the Cu-ZSM-5 ion exchange with iron. We carried out mechanistic studies with the expectation that we might get additional insights into synergistic effects of heteroatom incorporation and possibly comment on the structure. Our studies build on previous mechanistic studies including the report from Sachtler *et al*. on NO adsorption on Fe-MFI[41] and BaNa-Y[42], and from Chen *et al*.[43] on differences between copper and iron based zeolite (ZSM-5) in the $NH_3$ SCR.

After the initial contact with $NO_x/O_2$ (Step 1) at 150°C, Cu-SSZ-13 displays (Figure 5.1A) peaks at 1574, 1595, and 1625 $cm^{-1}$, which can be assigned to nitrite/nitrate adsorbed on zeolites[41] and gradually increase in intensity as a function of time. In addition, a fast-growing peak is observed at 2160 $cm^{-1}$ accompanied by a second peak at 2185 $cm^{-1}$ after 2 minutes. Both merge to a broad double-shouldered peak centered at 2170 $cm^{-1}$, which from previous studies, can be assigned to $NO^+$ either adsorbed on zeolites or compounded with $NO_2/N_2O_4$.[42,44,45]

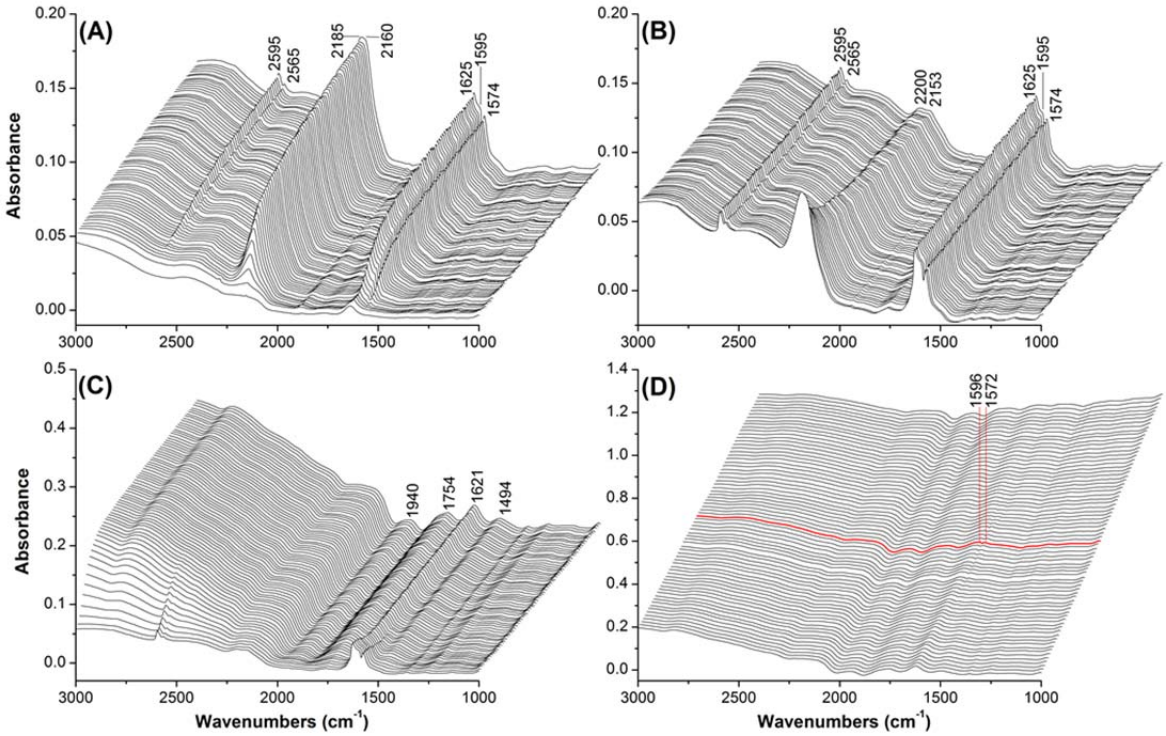


**Figure 5.1.** DRIFTS spectra of Cu-SSZ-13 at 150°C during the 4-step treatment (A. $NO_x/O_2$ flow, B. He purging, C. $NH_3/O_2$ flow, and D. desorption in He with temperature ramping to 600°C. Each step takes 15 minutes).

If $NO_2$ and $O_2$ are excluded from the gas input, the 2170cm$^{-1}$ peak is suppressed and the peaks associated with $NO_2$ are not observed (Figure 5.2). Low intensity peaks at 2565 and 2595 cm$^{-1}$ (with a broad shoulder) are also observed and assigned to adsorbed nitrates/nitrites due to the synchronic behavior to those fully identified peaks associated with nitrates/nitrites at 1574, 1595, and 1625 cm$^{-1}$. After replacing $NO_x/O_2$ flow with He, the nitrate/nitrite peaks (1574, 1595, and 1625 cm$^{-1}$), as well as the low intensity peaks at 2565 and 2595 cm$^{-1}$, remain unchanged but the 2170 cm$^{-1}$ peak is completely depleted suggesting weak adsorption nature of the $NO^+$ species on zeolite surface (Figure 5.1B). Also, the nitrate/nitrite peak heights (1574, 1595, and 1625 cm$^{-1}$) remain unchanged during thermal treatment up to 500°C (Figure 5.3).

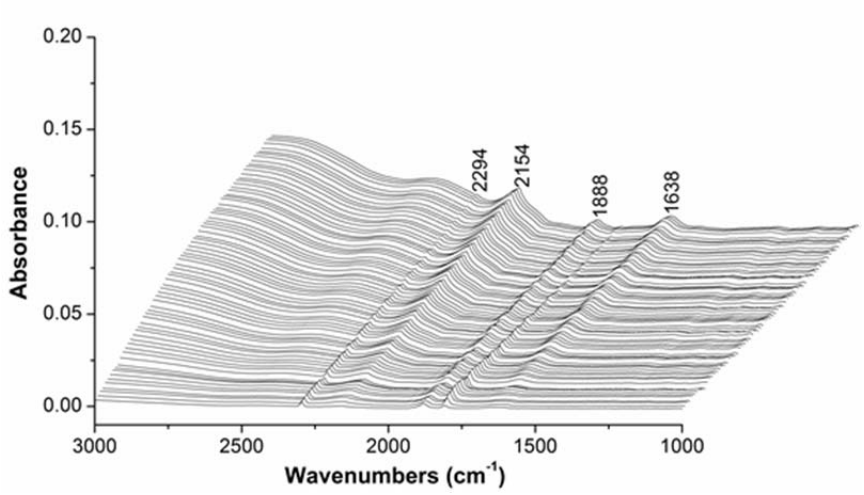


**Figure 5.2.** DRIFTS spectra of Cu-SSZ-13 at 150°C under a flow of NO (250 ppm) and He (balance) for 15 minutes.

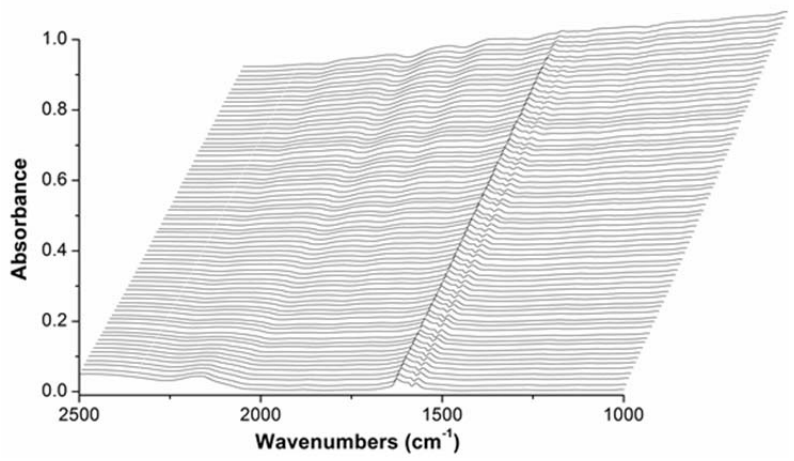


**Figure 5.3.** DRIFTS spectra of $NO^+$ and nitrite/nitrate adsorbed over Cu-SSZ-13 during the heating process from 150°C to 500°C (20°C/min) under a flow of He. Time interval between two spectra is 0.02 minute.

After ammonia flow is started, there is time delay of ~1 minute before the depletion of nitrate/nitrite associated peaks at 1574 and 1595 $cm^{-1}$ (Figure 5.1C). This suggests that $NH_3$ is adsorbed by the zeolite skeleton until saturation before arriving at the active metal sites for catalysis. The nitrate/nitrite peaks completely vanish by the end of the ammonia treatment cycle. At the end of ammonia treatment cycle, the spectrum resembles the spectrum of ammonia treated parent zeolite (Figure 5.4) and the four adsorption peaks between 1400 and 2000 $cm^{-1}$ are due to strongly adsorbed $NH_3$ species. The intensity of these peaks does not change even after heating to 600°C in the flow of He in the last step (Figure 5.1D). During heating in the last step (Figure 6D), two peaks at 1572 and 1596 $cm^{-1}$ reappear at about 300°C suggesting the presence of adsorbed nitrate/nitrite. This must occur due to the migration of $NO_x$ from inactive sites in the zeolite structure to catalytically active sites. As adsorbed ammonia reaches these sites also, the formation of $N_2$ and $H_2O$ is observed from the online mass spectrometry due to $NO_x$ reduction.

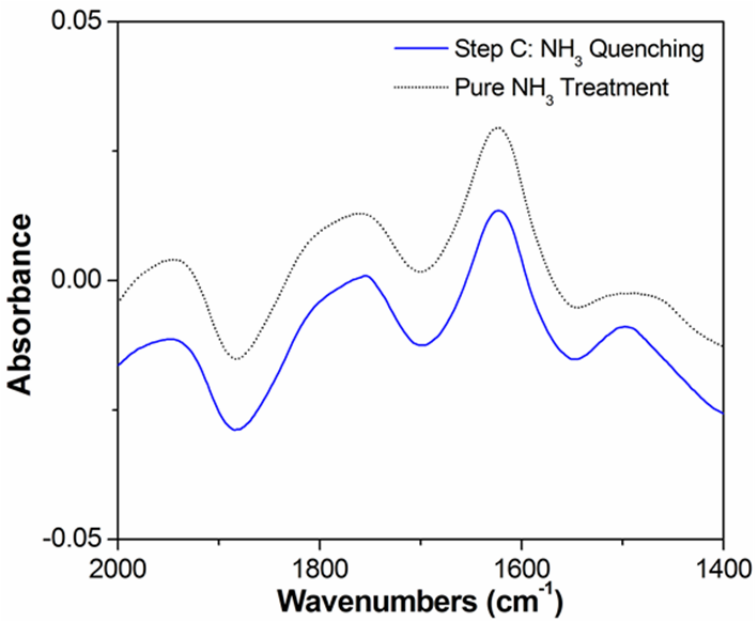


**Figure 5.4.** DRIFTS spectra comparison of Cu-SSZ-13 between two conditions: (1) a flow of $NH_3$ (500 ppm) and He (balance) for 15 minutes (dotted line) and (2) the third step treatment of $NH_3$ (500 ppm), $O_2$ (8.5%), and He (balance) for 15 minutes (solid line)

Increasing the $NO_x/O_2$ reaction temperature to 250°C results in no significant change except the $NO^+$ species peaks are less intense than those for nitrite/nitrate and additional weak bands are observed at 1389, 1357, and 1256 $cm^{-1}$ (Figure 5.5A), previously assigned to surface nitrate/nitrite.[42] The He cleaning step results in a faster disappearance of $NO^+$ species peaks (Figure 5.5B) but the weak bands at 1389 1357, and 1256 $cm^{-1}$ remain unchanged.

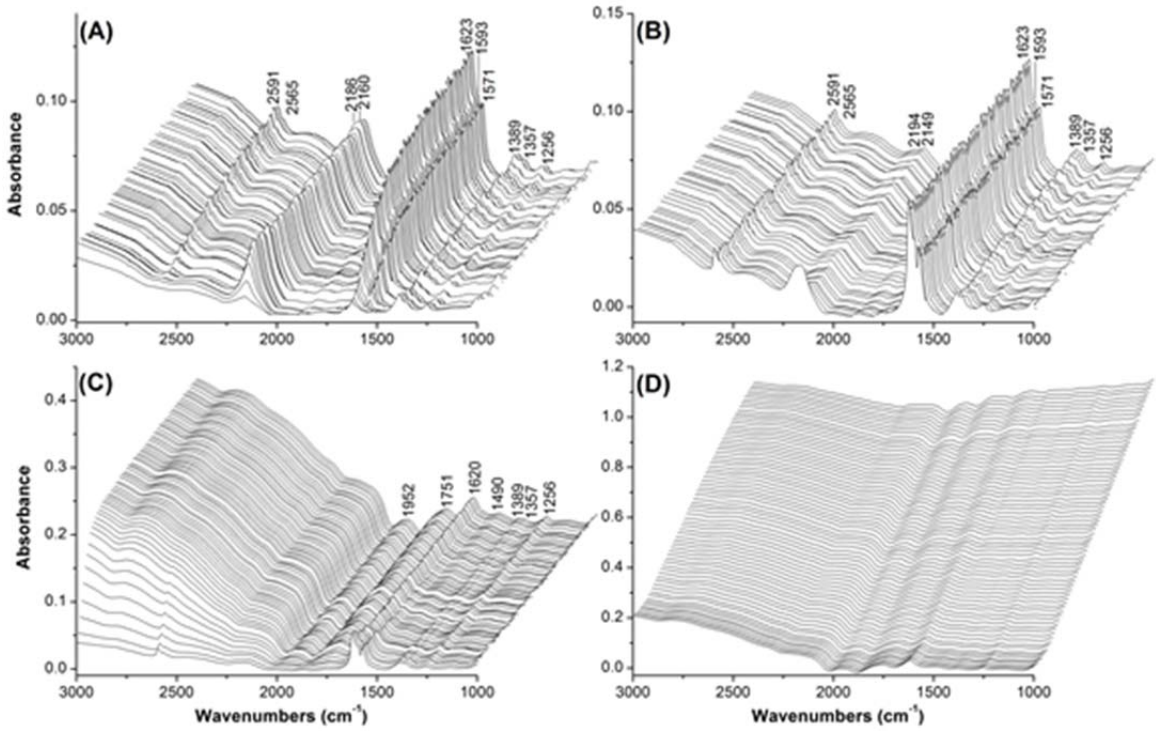


**Figure 5.5.** DRIFTS spectra of Cu-SSZ-13 at 250°C under the 4-step treatment (A. $NO_x/O_2$ flow, B. He purging, C. $NH_3/O_2$ flow, and D. desorption in He with temperature ramping to 600°C. Each step takes 15 minutes).

The spectrum of the new catalyst, CuFe-SSZ-13, is almost identical to Cu-SSZ-13 during all four steps of treatment at 150°C except that the $NO^+$ peak is nearly twice in intensity for CuFe-SSZ-13 (Figure 5.6) and a higher proportion of this peak remains after He purge step (Figure 5.7B). A slight enhancement in the intensity of peak at 1881 $cm^{-1}$ is also observed. Increasing the $NO_x/O_2$ reaction temperature to 250°C in step I makes the IR spectra on CuFe-SSZ-13 identical to those on Cu-SSZ-13(Figure 5.8). Thus, it is possible that there is a correlation between high $NO_x$ reduction activity and the enhanced of $NO^+$ formation at 150°C. Since $NO^+$ species is retained even after He purge, it is probably linearly bound to Cu center in a weak mode rather than being present only in the gas phase as suggested by Sachtler *et al*.[42]

Thus, our results suggest that $NO^+$ plays an important role in fast SCR reaction, and the high catalytic activity of heterobimetallic zeolites at 150°C can be attributed to the high $NO^+$ concentration as compared with monometallic zeolites. This is in contrast with earlier postulation[41,42] that attributed $NO_x$ reduction under fast SCR conditions to $N_2O_3$, which can form as an intermediate in the gas phase equilibrium of NO + $NO_2$, and can react with 2 equivalent of $NH_3$ to yield ammonium nitrite ($NH_4NO_2$) that decomposes to $N_2$ and $H_2O$ near 100°C.

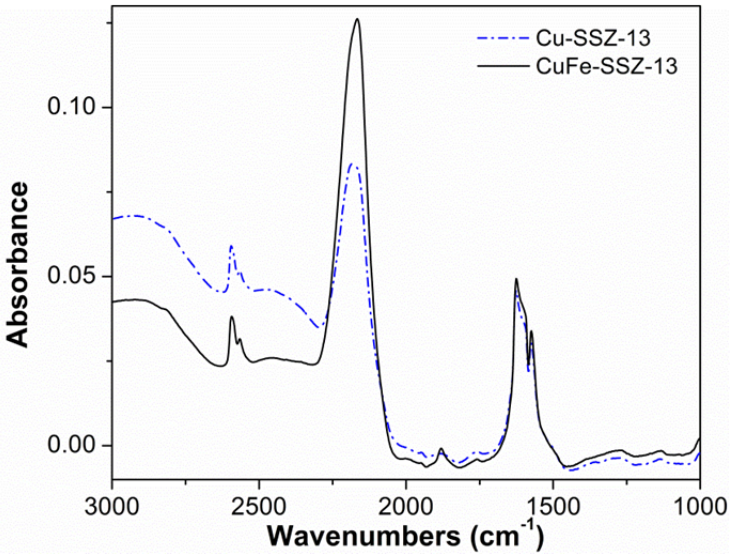


**Figure 5.6.** DRIFTS spectra of CuFe-SSZ-13 vs. Cu-SSZ-13 treated by $NO_x/O_2$ at 150°C.

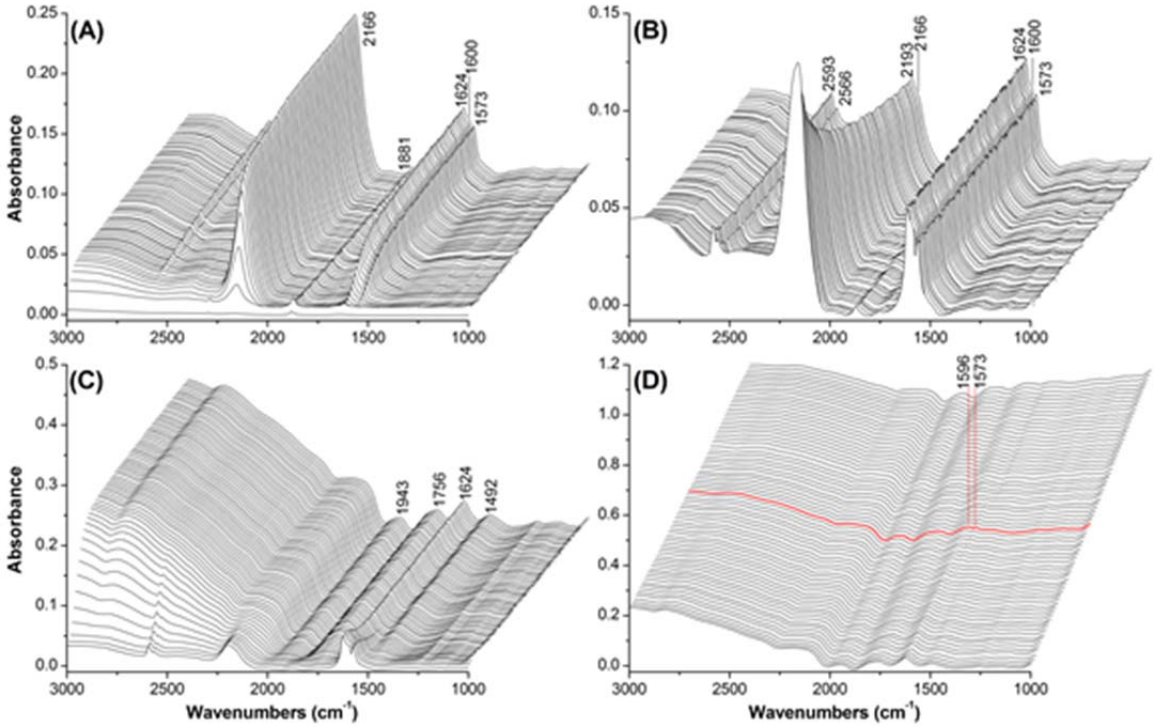


**Figure 5.7.** DRIFT spectra of CuFe-SSZ-13 at 150°C during the 4-step treatment (A. $NO_x/O_2$ flow, B. He purging, C. $NH_3/O_2$ flow, and D. desorption in He with temperature ramping to 600°C. Each step takes 15 minutes).

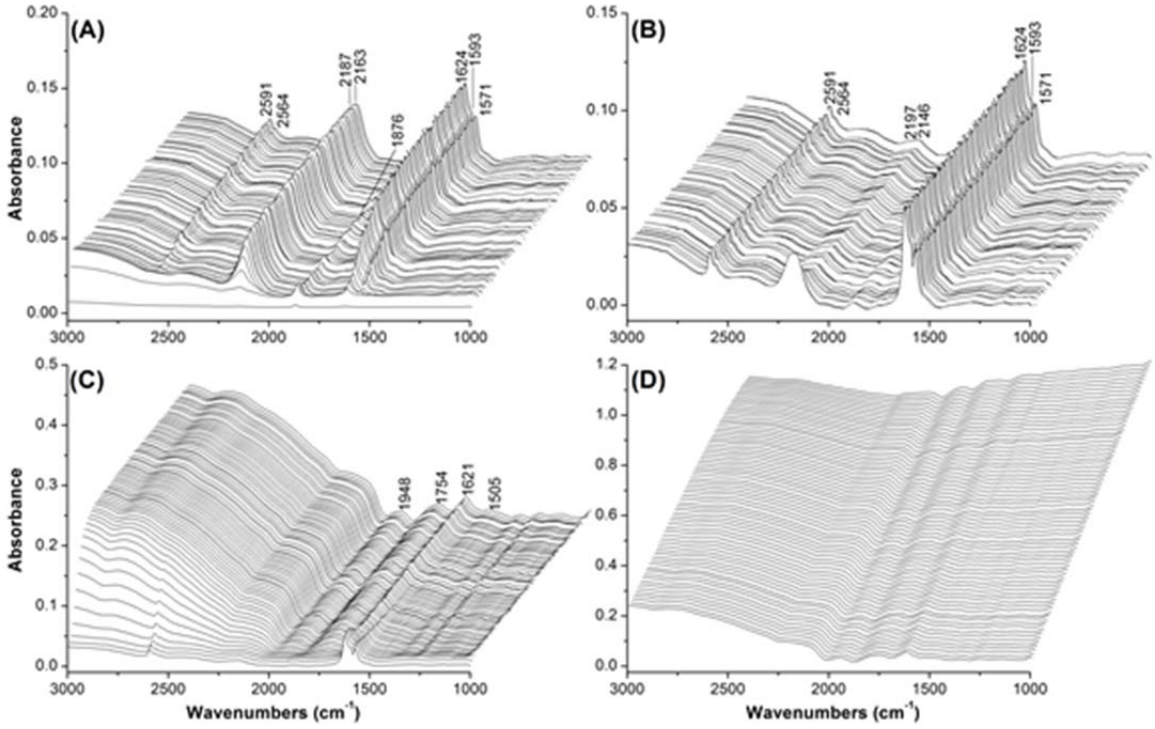


**Figure 5.8.** DRIFTS spectra of CuFe-SSZ-13 at 250°C under the 4-step treatment (A. $NO_x/O_2$ flow, B. He purging, C. $NH_3/O_2$ flow, and D. desorption in He with temperature ramping to 600°C. Each step takes 15 minutes).

In our study, the formation of $N_2O_3$ with IR peaks at 1879, 1578, and 1297 $cm^{-1}$ as reported by Sachtler,[41] is not dominant. The generation of adsorbed $NO^+$ species has been shown by Sachtler *et al*,[42] who suggested that $N_2O_4$, a dimer of $NO_2$, disproportionate to $NO^+$ and $NO_3^-$ over the catalyst. Our results are more aligned with this observation. The pathway of $NO^+$ reduction by $NH_3$ to $N_2$ has been proposed by previous theoretical[46-50] and experimental[51-53] studies to involve instable intermediate nitrosamide, $H_2NNO$. The overall fast-SCR reaction scheme can be summarized as follows (Figure 5.9A):

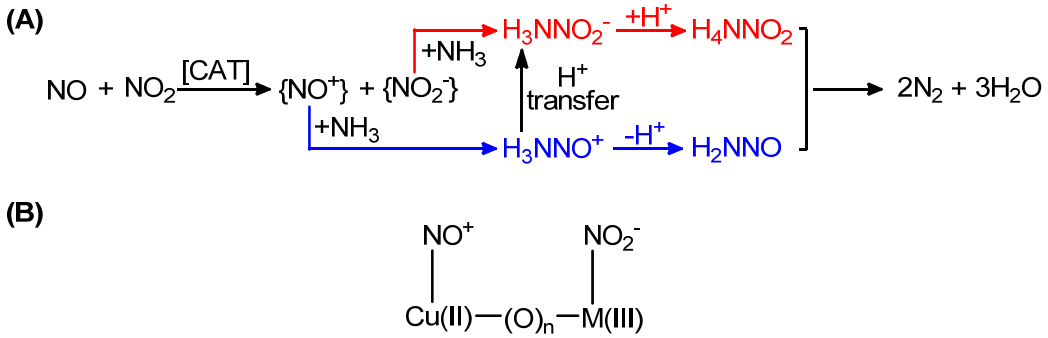


**Figure 5.9.** Fast-SCR reaction intermediates

The enhanced $NO_x$ reduction at 150°C by heterobimetallic zeolites must originate from the higher concentrations of $NO^+$ at 150°C, while nitrite/nitrate formation remains unchanged as compared with parent monometallic zeolites. It is likely that the enhanced $NO^+$ generation occurs at the Cu sites with high valence, i.e., Cu(III). $O_2$ may provide sufficient oxidation power to generate Cu(III) as demonstrated by a square planar copper complex.[54] Introduction of a redox active metal into the vicinity of the active copper center can strengthen the weak interaction between Cu(III) and the $NO^+$. In addition, a heterobimetallic site can promote the disproportionation reaction between NO and $NO_2$ (Figure 5.9B) even in the absence of an external oxidant to generate transient Cu(III) based on the asymmetric structure motif to gain additional free energy when compared to a homogeneous bimetallic core by hosting $NO_2^-$ at the higher charged metal M(III) and $NO^+$ at the Cu(II) site. These assumptions explain the dependence of the degree of low temperature $NO_x$ conversion on redox properties of heteroatom in our heterobimetallic zeolites where La, Fe, Sc, In incorporated zeolites exhibit 83, 79, 74, and 71% $NO_x$ conversion at 150°C, respectively.

## 6. CONCLUSIONS

In conclusion, we have shown that hydrothermally stable heterobimetallic zeolites can be easily prepared by ion exchange of monometallic zeolites. The heterobimetallic zeolites offer the additional advantage of low temperature $NO_x$ conversion activity as compared with the parent monometallic zeolites. Among various heterobimetallic zeolites synthesized during the course of this project, CuFe-SSZ-13 offers the best combination of $NO_x$ conversion performance in 150-650°C and hydrothermal durability under simulated operating conditions. **This result enabled us to meet both stated objectives of this project – wide operating temperature window and hydrothermal durability.**

The characterization data from diffuse-reflectance UV-Vis, XRD, EXAFS and EPR do not permit conclusive structural determination but support the proposal that $M^{3+}$ has been incorporated in the vicinity of Cu(II). The mechanistic studies suggest that the origin of low temperature reactivity is related to the production and retention of the $NO^+$ species. It is likely that a heterobimetallic core facilitates the disproportionation reaction between NO and $NO_2$ to form and stabilize $NO^+$ and $NO_2^-$.

The next steps will involve scale up and engine testing to facilitate commercialization of this technology.

## 7. COMMERCIALIZATION

The emission treatment catalysts go through a three-step development process after discovery – laboratory testing, engine testing (dynamometer testing), and on vehicle testing. If a catalyst demonstrates high performance through all three steps, it goes through certification procedure on a vehicle line before deployment.

In this report, we have summarized our results on the discovery and laboratory testing of a series of new heterobimetallic zeolite catalysts. Among these catalysts, CuFe-SSZ-13 exhibits the best combination of wide temperature operating window (150-650C) and hydrothermal durability. The performance a low temperature is far better than the current commercial catalyst Cu-SSZ-13.

The next step will involve getting CuFe-SSZ-13 loaded on a honeycomb substrate and engine testing under NH3-SCR conditions. Depending on the results, we would also like to evaluate performance under Federal Test Protocol (FTP).

The successful demonstration of engine testing will make it a marketable technology. As listed in the publication section, we have filed two patents based on the work described in this report.

# 8. PUBLICATIONS

US Patents

Narula, C.K.; Yang, X.; Zeolite Based SCR Catalysts for Off-Road Diesel Engine Emission Treatment, US Patent Application 12855794, August 13, 2010.

Narula, C.K.; Yang, X.; Hydrothermally Stable, Low-Temperature $NO_x$ Reduction $NH_3$-SCR Catalyst, Invention Disclosure Number 2011-02721

Publications

Yang, X.; Narula, C.K.; A Simple Approach for Tuning Catalytic Activity of MFI-Zeolites for Low-Temperature $NO_x$ Reduction, (Manuscript in preparation)

Yang, X.; Bonnesen, P.V.; Narula, C.K.; High Performance $NH_3$ SCR Zeolite Catalysts for Treatment of $NO_x$ in Emissions from Off-Road Diesel Engine, SAE-2011-01-1330

Presentations

Yang, X; Buchanan, A.C., Kidder, M.; Hageman, E; Narula, C.K.; Heterobimetallic zeolites: Synthesis, characterization, and applications, American Chemical Society National Meeting, March 2011, Denver, Co.

Yang, X.; Narula, C.K.; High Performance $NH_3$-SCR Zeolite Catalysts for Treatment of $NO_x$ in Emissions from Diesel Engines, SAE world congress 2011-01-0071 presentation on April 13, 2011.

Yang, X; Buchanan, A.C., Kidder, M.; Hageman, E; Narula, C.K.; Heterobimetallic zeolites: Synthesis, characterization, and applications, American Chemical Society National Meeting, March 2011, Anaheim, CA.

Yang, X.; Narula, C.K.; A Simple Approach of Tuning Catalytic Activity of MFI-Zeolites for Low-Temperature SCR of $NO_x$, Directions in Engine-Efficiency and Emissions Research (DEER) Conference, Detroit, MI, September 27-30, 2010

Yang, X.; Narula, C.K.; High Performance $NH_3$-SCR Zeolite Catalysts for Treatment of $NO_x$ in Emissions from Diesel Engines, ACS National Meeting, Boston, August 22-26, 2010

## 9. REFERENCES


(1) *Introduciton to Zeolite Science and Practice*, 3rd ed.; Elsevier: Amsterdam, 2007.
(2) Tanabe, K.; Holderich, W. F. *Appl. Catal. A* **1999**, *181*, 399-434.
(3) Palella, B. I.; Lisi, L.; Pirone, R.; Russo, G.; Notaro, M. *Kinet. Catal.* **2006**, *47*, 728-736.
(4) Joyner, R.; Stockenhuber, M. *J. Phys. Chem. B* **1999**, *103*, 5963-5976.
(5) Zecchina, A.; Rivallan, M.; Berlier, G.; Lamberti, C.; Ricchiardi, G. *Phys. Chem. Chem. Phys.* **2007**, *9*, 3483-3499.
(6) Guisnet, M.; Gnep, N. S.; Alario, F. *Appl. Catal. A* **1992**, *89*, 1-30.
(7) Cantin, A.; Corma, A.; Diaz-Cabanas, M. J.; Jorda, J. L.; Moliner, M. *J. Am. Chem. Soc.* **2006**, *128*, 4216-4217.
(8) Hong, S. B.; Uh, Y. S.; Woo, S. I.; Lee, J. K. *Korean J. Chem. Eng.* **1991**, *8*, 1-5.
(9) Liu, X. S.; Klinowski, J. *J. Phys. Chem.* **1992**, *96*, 3403-3408.
(10) Woertink, J. S.; Smeets, P. J.; Groothaert, M. H.; Vance, M. A.; Sels, B. F.; Schoonheydt, R. A.; Solomon, E. I. *Proc. Natl. Acad. Sci. USA* **2009**, *106*, 18908-18913.
(11) Komatsu, T.; Nunokawa, M.; Moon, I. S.; Takahara, T.; Namba, S.; Yashima, T. *J. Catal.* **1994**, *148*, 427-437.
(12) Iwamoto, M.; Furukawa, H.; Mine, Y.; Uemura, F.; Mikuriya, S. I.; Kagawa, S. *J. Chem. Soc., Chem. Commun.* **1986**, 1272-1273.
(13) Long, R. Q.; T., Y. R. *J. Am. Chem. Soc.* **1999**, *121*, 5595-5596.
(14) Komatsu, T.; Uddin, M. A.; Yashima, T. *Zeolite: A Refined Tool for Designing Catalytic Sites*; Elsevier: Amsterdam, 1995.
(15) Devadas, M.; Krocher, O.; Elsener, M.; Wokaun, A.; Mitrikas, G.; Soger, N.; Pfeifer, M.; Demel, Y.; Mussmann, L. *Catal. Today* **2007**, *119*, 137-144.
(16) Cavataio, G.; Girard, J.; Patterson, J.; Montreuil, C.; Cheng, Y.; Lambert, C., SAE Paper # 07PFL-643.
(17) Cavataio, G.; Jen, H. W.; Warner, J. R.; Girard, J. W.; Kim, J. Y.; Lambert, C. K., SAE Paper # 08PFL-723.
(18) Bull, I.; Xue, W.; Burk, P.; Boorse, S. R.; Jaglowski, W. M.; Koermer, G. S.; Moini, A.; Patchett, J. A.; Dettling, J. C.; Caudle, M. T. *United States Patent* **2009**, 7601662.
(19) Korhonen, S. T.; Fickel, D. W.; Lobo, R. F.; Weckhuysen, B. M.; Beale, A. M. *Chem. Commun.* **2011**, *47*, 800-802.
(20) Kwak, J. H.; Tonkyn, R. G.; Kim, D. H.; Szanyi, J.; Peden, C. H. F. *J. Catal.* **2010**, *275*, 187-190.
(21) Kieger, S.; Delahay, G.; Coq, B.; Neveu, B. *J. Catal.* **1999**, *183*, 267-280.
(22) Amiridis, M. D.; Puglisi, F.; Dumesic, J. A.; Millman, W. S.; Topsoe, N. Y. *J. Catal.* **1993**, *142*, 572-584.
(23) Deng, H. B.; Hoffmann, R. *Angew. Chem. Int. Ed.* **1993**, *32*, 1062-1065.
(24) Baik, M. H.; Newcomb, M.; Friesner, R. A.; Lippard, S. J. *Chem. Rev.* **2003**, *103*, 2385-2419.
(25) Zones, S. I. *United States Patent* **1985**, 4544538.
(26) Fickel, D. W.; Fedeyko, J. M.; Lobo, R. F. *J. Phys. Chem. C* **2010**, *114*, 1633-1640.
(27) Axon, S. A.; Klinowski, J. *J. Phys. Chem.* **1994**, *98*, 1929-1932.

(28) Ismagilov, Z. R.; Yashnik, S. A.; Anufrienko, V. F.; Larina, T. V.; Vasenin, N. T.; Bulgakov, N. N.; Vosel, S. V.; Tsykoza, L. T. *Appl. Surf. Sci.* **2004**, *226*, 88-93.
(29) Kucherov, A. V.; Slinkin, A. A.; Kondratev, D. A.; Bondarenko, T. N.; Rubinstein, A. M.; Minachev, K. M. *Zeolites* **1985**, *5*, 320-324.
(30) Grunert, W.; Hayes, N. W.; Joyner, R. W.; Shpiro, E. S.; Siddiqui, M. R. H.; Baeva, G. N. *J. Phys. Chem.* **1994**, *98*, 10832-10846.
(31) Teraishi, K.; Ishida, M.; Irisawa, J.; Kume, M.; Takahashi, Y.; Nakano, T.; Nakamura, H.; Miyamoto, A. *J. Phys. Chem. B* **1997**, *101*, 8079-8085.
(32) Koebel, M.; Elsener, M.; Madia, G. *Ind. Eng. Chem. Res.* **2001**, *40*, 52-59.
(33) He, Z.; He, C.; Gao, E. Q.; Wang, Z. M.; Yang, X. F.; Liao, C. S.; Yan, C. H. *Inorg. Chem.* **2003**, *42*, 2206-2208.
(34) Maensiri, S.; Laokul, P.; Klinkaewnarong, J.; Phokha, S.; Promarak, V.; Seraphin, S. *Optoelectron Adv. Mat.* **2008**, *2*, 161-165.
(35) Liu, G. *Int. J. Electrochem. Sci.* **2011**, *6*, 2162-2170.
(36) Brandenberger, S.; Krocher, O.; Tissler, A.; Althoff, R. *Catal Rev* **2008**, *50*, 492-531.
(37) Suzuki, K.; Sano, T.; Shoji, H.; Murakami, T.; Ikai, S.; Shin, S.; Hagiwara, H.; Takaya, H. *Chem. Lett.* **1987**, 1507-1510.
(38) Sano, T.; Suzuki, K.; Shoji, H.; Ikai, S.; Okabe, K.; Murakami, T.; Shin, S.; Hagiwara, H.; Takaya, H. *Chem. Lett.* **1987**, 1421-1424.
(39) Kröcher, O.; Devadas, M.; Elsener, M.; Wokaun, A.; Soger, N.; Pfeifer, M.; Demel, Y.; Mussmann, L. *Appl. Catal. B-Environ.* **2006**, *66*, 208-216.
(40) Rahkamaa-Tolonen, K.; Maunula, T.; Lomma, M.; Huuhtanen, M.; Keiski, R. L. *Catal. Today* **2005**, *100*, 217-222.
(41) Sun, Q.; Gao, Z. X.; Chen, H. Y.; Sachtler, W. M. H. *J. Catal.* **2001**, *201*, 89-99.
(42) Yeom, Y. H.; Henao, J.; Li, M. J.; Sachtler, W. M. H.; Weitz, E. *J. Catal.* **2005**, *231*, 181-193.